



Hole transport layers in organic solar cells: A review

Riva ALKARSIFI¹, Jörg ACKERMANN¹, and Olivier MARGEAT^{1,*}

¹ Aix Marseille Univ, CNRS, CINaM, Marseille, France

*Corresponding author e-mail: olivier.margeat@univ-amu.fr

Received date:

7 November 2022

Revised date

12 December 2022

Accepted date:

13 December 2022

Keywords:

Organic solar cell;
Interfaces;
Hole transporting layer

Abstract

Thanks to huge research efforts, organic solar cells have become serious candidates in the field of renewable energy sources, with reported power conversion efficiencies above 19% and operating lifetime surpassing decades. In the thin film stack composing the organic solar cell, the transport layers at interfaces play a key role, as important as the photoactive material itself. Both electron (ETL) and hole (HTL) transport layers are indeed directly involved in the efficiency and stability of the devices, due to the very specific properties required for these interfaces. Focusing on the HTL interface, a large number of materials has been used in organic solar cells, such as 2D materials, conductive polymers or transition metal oxides. In this review, we present the evolution and recent advances in HTL materials that have been employed in manufacturing organic solar cells, by describing their properties and deposition processes, and also relating their use with the fullerene or the new non-fullerene acceptors in the active layer.

1. Introduction

Solar cells, or photovoltaic cells, without any doubt, can be considered as one of the important energy conversion devices converting solar energy directly into electric energy using the photovoltaic effect. They are described as being photovoltaic (PV), irrespective whether the light source is sunlight or an artificial light [1]. The third generation of solar cells known as emerging photovoltaics constitutes a number of thin-film technologies including (i) dye sensitized solar cells (DSSC), also called Grätzel cells which are electrochemical cells with an electrolyte.[2] It includes as well (ii) Perovskite solar cells and Quantum dots (QDs) hybrid solar cells in addition to (iii) organic photovoltaics (OPV) which are made up of semiconducting donor and acceptor composite. Although organic solar cells (OSCs) are still plagued by issues related to their power conversion efficiency (PCE) and stability, lots of researches focus on this promising technology as they believe that they can achieve low-cost and high efficiency organic solar cells at large scales.

Taking a closer look at organic photovoltaic field, a SWOT analysis can be conducted in order to help assess the technology's potential nowadays. In this analysis, the strengths and weaknesses of the OPV technology are discussed. Furthermore, future market opportunities and threats can be analyzed to see how well OPVs will be placed in the market landscape. One of the major strengths which OPVs have against other solar panels is their semi-transparency. This allows them to be used for numerous novel applications as window tints, smartphone screen covers and others. Another strong advantage is their light weight when compared to single and multi-silicon photovoltaics on the current market. They are among the most promising approaches thanks to their flexibility solution processability and low costs compared to regular inorganic technologies. Organic solar cells are

known to be environmental friendly with less environmental impact during manufacturing and operation [3]. They are the only solar cell technology that fully addresses the challenges of large scale production, being manufactured by some printing techniques like ink-jet printing and Roll to Roll processes [4]. Today, fully printed prototypes are manufactured and first products are available [5].

On the contrary, organic solar cells are still limited by their lower efficiency when compared to silicon-based photovoltaics. While the latter devices reached an efficiency above 20%, organic solar cells are still facing some challenges limiting their efficiency to around 19.05%.[6] Another weakness of the OPV market is their weak stability. Currently, the OPVs being sold in markets will maintain their efficiencies for a maximum of 2 years. In contrast, silicon-based photovoltaics can maintain their efficiencies for twenty plus years. The stability of organic solar cells is often limited by the metastable bulk-heterojunction morphology which is sensitive to oxygen and moisture, the diffusion of the electrode and the interfacial layers (ILs) sandwiching the photoactive layers [7]. However, recent works show that OSCs can retain their efficient bulk-heterojunction morphology, using appropriate materials and careful choice of interfaces, claiming performance stability as high as 30 years.[8]

Many opportunities are present for OPV technologies to fall into a niche market category if the panels were developed to be more efficient comparable to silicon-based photovoltaics. Building Integrated Photovoltaics is a market sector which can help OPV market to grow. Flexible OPV laminates can be integrated into glass facades, curtain walls, roofs and many other surfaces. Architects can play around with transparency and color. This means we are no longer limited to the rigidity and the black color of silicon solar panels. Future possibilities might be organic charging tablets and laptop screens [9]. Meanwhile, OPVs will continue to face some threats within the next couple of

years due to the competition with silicon solar cells that occupy around 90% of sales markets. With more researches on organic photovoltaic, we can hope for an increase in efficiency and sustainability in the near future. [10], [11]

2. Concept of solar cells

2.1 Device architecture

OSC is a stack of multilayers as shown in Figure 1. It is built on a transparent substrate coated with a conductive and transparent electrode material allowing light to pass through. Due to the excellent transparency and conductivity of indium tin oxide (ITO), it has been broadly employed as one of the electrodes.

The light harvesting layer known as the photoactive layer is made up of donor and acceptor molecules. Donors are usually conjugated polymers, oligomers or conjugated pigments example poly(3-hexylthiophene) (P3HT), poly({4,8-bis[(2-ethylhexyl)oxy]benzo[1,2-b:4,5-b']dithiophene-2,6-diyl}{3-fluoro-2-[(2-ethylhexyl)carbonyl]thieno[3,4-b]thiophenediyl})(PTB7), poly([2,6'-4,8-di(5-ethylhexylthienyl)benzo[1,2-b:3,3-b]dithiophene]{3-fluoro-2[(2-ethylhexyl)carbonyl]thieno[3,4-b]thiophenediyl})(PTB7-Th or PCE-10), while acceptors could be either fullerene derivatives like [6,6]-Phenyl C₆₁ butyric acid methyl ester (PC60BM) and [6,6]-Phenyl C₇₁ butyric acid methyl ester (PC70BM) or non-fullerene acceptors (NFAs) that can be small molecules for example 2,2'-[[6,6,12,12-Tetrakis(4-hexylphenyl)-6,12-dihydro dithieno [2,3-d:2',3'-d']-s-indaceno[1,2-b:5,6b']dithiophene-2,8 diyl]bis[methyldiyn-(3-oxo-1H-indene-2,1(3H)-diylidene)]]bis[propane dinitrile] (ITIC) and its derivatives. The chemical structures of some donors and

acceptors are shown in Figure 2. These materials are often classified as organic semiconductors. The photoactive layer is normally sandwiched between two interfacial layers, a hole transport layer (HTL) and an electron transport layer (ETL). On the top is the metal electrode which is also used for charge collection [3]. Depending on the device structure (regular or inverted), the top metal electrode could be either anode or cathode. For an efficient charge collection, the work functions (WF) of both electrodes, anode and cathode, should match the highest occupied molecular orbital (HOMO) of the donor and the lowest unoccupied molecular orbital (LUMO) of the acceptor, respectively [12]. ITO is in principle able to collect both positive (holes) and negative (electrons) carriers, because of the position of its work function with respect to the energy levels of both donors and acceptors [13].

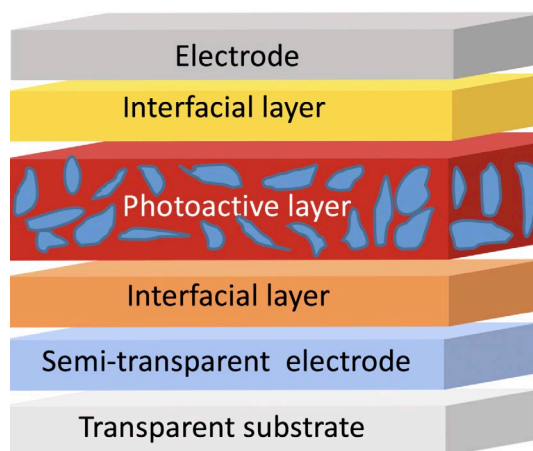


Figure 1. The basic structure of an organic solar cell.

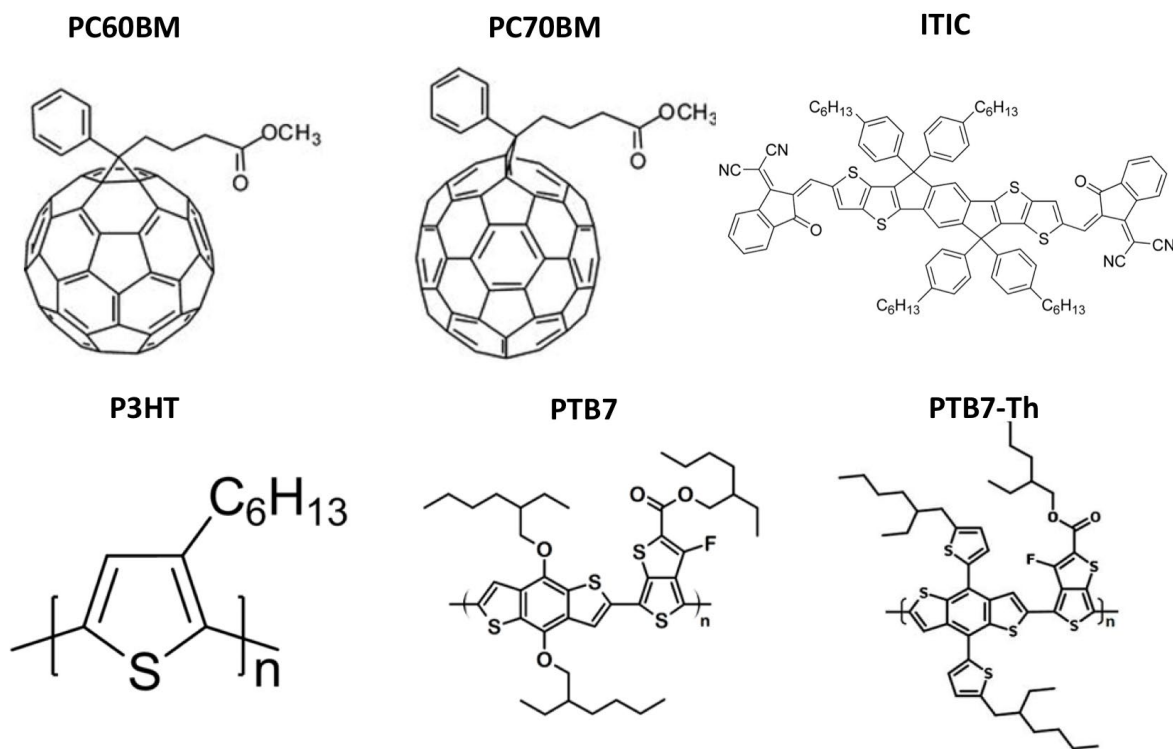


Figure 2. Chemical structures of some donors and acceptors used in OSCs.

Beside the active materials, the device structure is also important. In general, there are two main structures of OSCs: “the regular” device structure (also called normal or conventional structure) and the “inverted” device structure. The difference between the two structures is in the sequence of electrodes.

The regular-based devices consist of a glass substrate covered with a high work function semi-transparent conducting metal oxide as an anode. The most frequently used is ITO or fluorine doped tin oxide (FTO). The photoactive bulk heterojunction layer is sandwiched between a hole extraction layer mainly an acidic polymer named poly(3,4-ethylenedioxythiophene)-poly(styrenesulfonate) (PEDOT:PSS) and an electron extraction layer. Devices are completed with a non-transparent metal electrode of a low WF functioning as a cathode like aluminum (Al) and calcium (Ca).

In regular-based devices, PEDOT:PSS layer can cause corrosion to the ITO electrode. Additionally, the top metal electrode can be easily oxidized in air. During the vacuum evaporation deposition, micropores can be formed within the top metal electrode. This causes oxygen and moisture to be diffused into the photoactive layer leading to a rapid degradation of the underlying polymer. All these aspects will reduce the stability of the solar devices [14]. Moreover, it has been widely reported that polymer:fullerene blends are characterized by a stratified composition (vertical phase separation) during film formation, where the electron-conducting phase (acceptor) is mainly concentrated at the bottom of the film and the hole-conducting one (donor) is mainly concentrated at the top of the film. This structure is opposite to the ideal one, in which the acceptor must face the top low-work function electrode and the donor must face the bottom high work function electrode [15]; a phenomena which may result in low open-circuit voltage (V_{oc}).

Inverted device structure

In order to circumvent the above problems and improve device stability, the inverted device structures have been developed. In this device structure, the polarity of charge collection is reversed where ITO acts as a cathode to collect electrons and the high work function, air-stable metals such as silver (Ag) or gold (Au) are used as the top anode to collect holes, thus eliminating any oxidation problem. The transparent electron conducting layer can be metal oxides, like zinc oxide (ZnO) or titanium oxide (TiO_x), eliminating the problem of the acidic PEDOT:PSS on ITO or FTO.[16] OPVs based on inverted device structures do not only have superior ambient stability but also possess better compatibility to all-solution roll-to-roll processing since metal anodes can be deposited from commercially available colloidal solutions. Figure 3 shows the regular and inverted device structures used for OSCs.

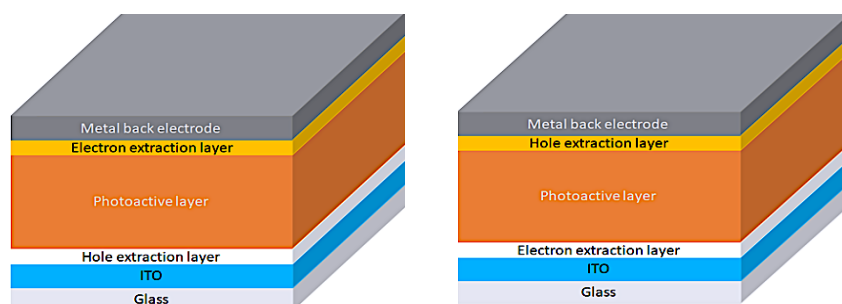


Figure 3. Typical regular (left) and inverted (right) device structures.

The first organic solar cell with inverted structure was prepared by Shirakawa *et al.* [17] applying a compact ZnO hole blocking layer and a gold layer as top electrode. The inverted device structure was performed using a fullerene-based binary system of PTB7:PC70BM and showed an efficiency of 5.87% [18]. Among the highest recorded efficiencies for inverted device structures was 16.5% using a PBDB-TF:BTP-4Cl blend with an active area of 0.09 cm² [19].

2.2 Constituents of the photoactive blend

As previously mentioned, the photoactive layer is a blend of materials having specific criteria allowing them to be used as donor and acceptor molecules. These materials must be properly mixed to form a layer with an optimized morphology for efficient devices.

2.2.1 Criteria of acceptors

A good acceptor for OPV must, at a minimum, have a high electron affinity (EA) and a good electron transport property in films. Other desirable properties include sufficient solubility for solution processing, intense visible to near-infrared (IR) light absorption and appropriate energy levels for a given electron donor material. When blended with a conjugated polymer donor, they should have large nonplanar structures to promote nanoscale phase separation, charge separation and charge transport in films [20].

HOMO levels, leading to semiconducting behavior and strong interactions with visible and near-infrared (IR) light. An ideal donor is the one with high hole mobility and affinity, as well as enhanced absorption spectrum in the visible and near-IR region [21]. The crystallinity of a donor must also be taken into consideration as an important criterion. In general, the performance of an OSC highly depends on microphase separation between donors and acceptors in a photoactive layer. Photo-generated excitons have to diffuse into the interface of donor and acceptor, separate into free charges and then transport to the electrodes. Thus, a highly crystalline polymer can easily generate large domain sizes (>100 nm) in films, which is helpful for charge transport, but detrimental to exciton diffusion due to the limited lifetime of exciton. On the other hand, amorphous conjugated polymers tend to form mixed thin films, facilitating exciton diffusion into interfaces, but hampering charge transport to the electrode due to severe charge recombination. Thus, it is important to precisely control the crystallinity of conjugated polymers in order to realize a suitable micro-phase separation in BHJ thin films [22]. Impurities, both intrinsic to the polymer as well as extrinsic, will have a severe negative effect on device performances.

2.2.2 Criteria of donors

Donors in organic solar cells are mainly π -conjugated small molecules or polymers with a typical molecular structure of alternating electron-donating and electron-accepting blocks. This π -conjugation results in typical energy gaps of 1 eV to 3 eV between LUMO and

2.2.3 Blend morphology

Processing of organic BHJ layer at lab scale is mainly performed by spin coating a mixture of a polymer and an acceptor from a common solvent, which implies that the polymer should possess a good solubility in organic solvents in which the acceptor will also dissolve. The preparation of this mixture is governed by a specific ratio between both components. This ratio should be optimized to obtain a nanoscale interpenetrating film morphology with appropriate domain sizes for efficient exciton dissociation and charge generation, while maintaining a good balance between donors and acceptors as they normally have different mobilities to electrons and holes [23]. However, by simply processing the BHJ layer from a blend solution of donor and acceptor materials in a single solvent usually results in a morphology correlated with poor performance. Therefore, methodologies to obtain a favorable morphology by adjustments to processing have been extensively investigated, such as, thermal annealing [24], and solvent vapor annealing [25]. Among these strategies, processing with a solvent

additive in addition to the primary host solvent – an approach developed in the 2000s [26]: [27] – was found to be effective for controlling the BHJ morphology. Host solvents usually possess high solubility to both electron donor and acceptor molecules whereas additives have selective solubility to one of the components (mainly acceptors). These additives normally have higher boiling points than the host solvents. [28] Figure 4 presents some of the additive molecules that have been incorporated in BHJ processing.

For example, extensive researches were devoted to PTB7:PC70BM BHJ blends processed without and with 1,8-diodooctane (DIO) additive. Using DIO, the efficiency of devices was increased from 3.53% up to 8.18% [29]. This was explained by the reduced size of fullerene aggregates resulting in an enhanced intercalation of the fullerene in the polymer chain, thus, better donor-acceptor intermixing [30]. Another study revealed that the presence of DIO supports the formation of polymer and fullerene rich domains which are needed for charge transportation [31]. This effect was clearly illustrated by Ben Dkhil *et al.* [29] after analyzing the morphology of the film using Scanning Transmission Electron Microscopy combined with spatially resolved spectroscopic imaging (STEM-SI) as shown in Figure 5. For both PTB7:PC70BM and PTB7-Th:PC70BM systems, the optimized amount of DIO was 3% and any further increase in this amount will cause a drop in efficiency due to the less interconnected pure domains.

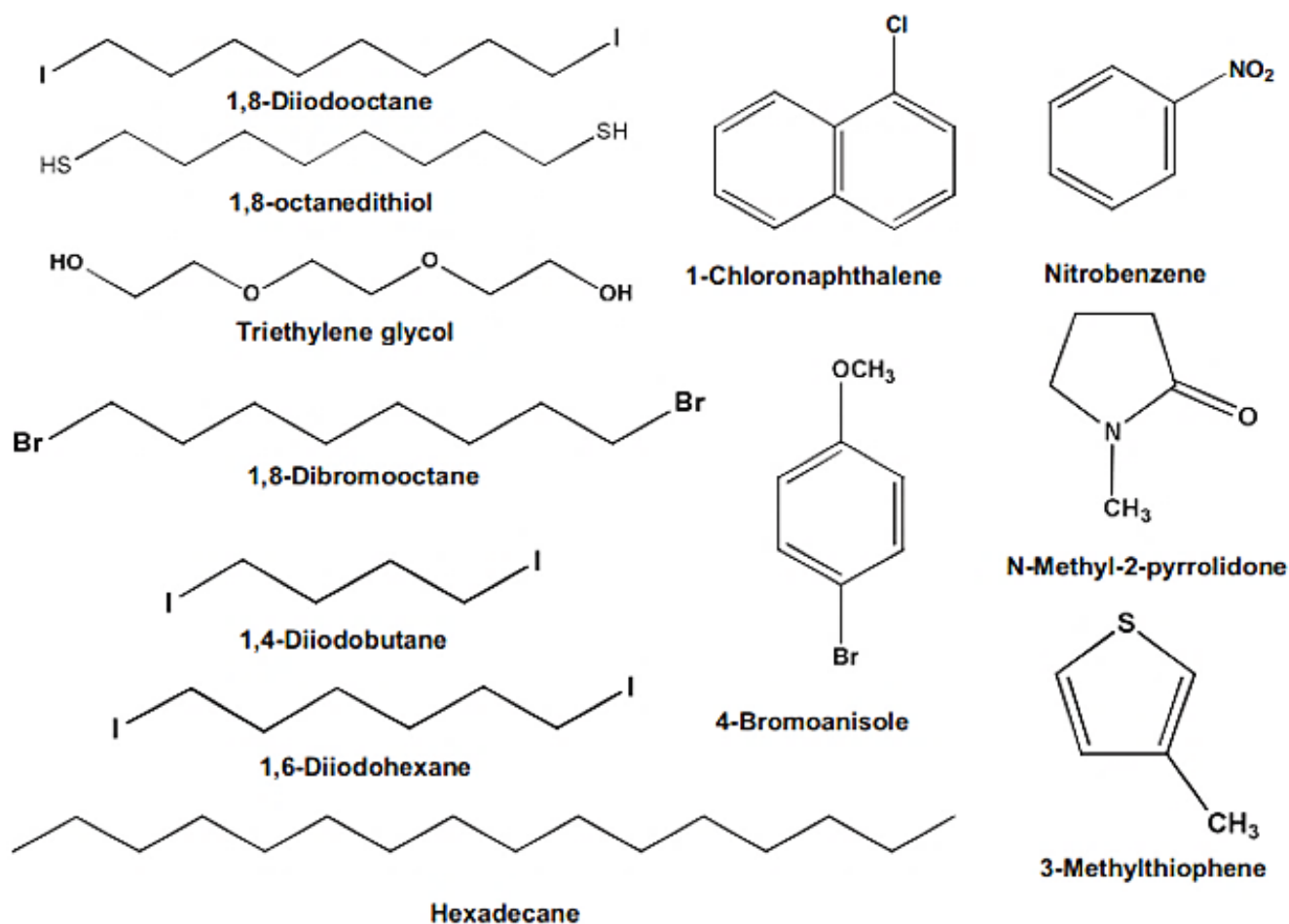


Figure 4. Examples of solvent additives for BHJ morphological control.

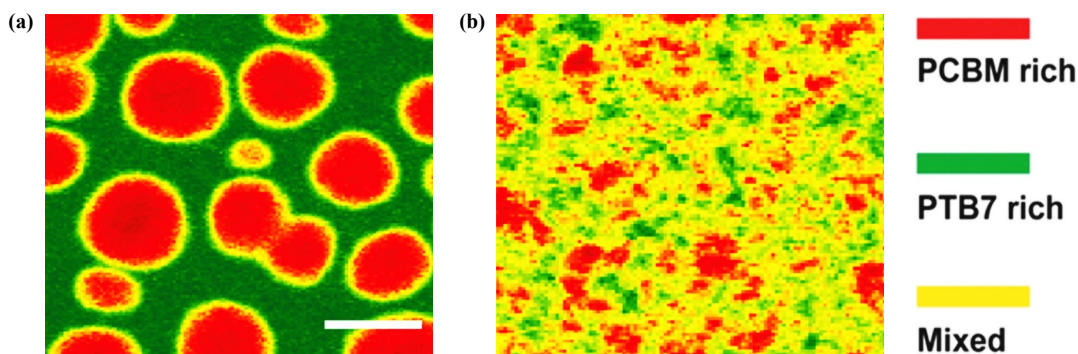


Figure 5. STEM-SI plasmon peak map of PTB7:PC70BM blends processed (a) without DIO and (b) with DIO. Reproduced from Ref. 29 with permission from Wiley Publishing Group.

2.3 Operating principle of OSCs

The working principle of bulk heterojunction (BHJ) devices can be described in few fundamental steps:

2.3.1 Light absorption and exciton generation

Sunlight is absorbed by a photoactive layer consisting of donor and acceptor semiconducting organic materials. Donor materials (D) donate electrons and mainly transport holes while acceptor materials (A) withdraw and transport electrons. Those photoactive materials harvest photons from sunlight to form excitons (tightly bound electron-hole pairs). In the bulk heterojunction, the number of p-n junction interfaces should reach a theoretical limit. The electrons are excited from the HOMO of a donor to its LUMO level -thanks to the energy input of the absorbed photon- leaving behind a hole or a positive charge in the HOMO level to maintain neutrality (Figure 6).

2.3.2 Exciton diffusion

Due to concentration gradient, excitons diffuse to the donor/acceptor interface (interfaces within diffusion length). Photo-generated excitons are characterized by a very small lifetime of few picoseconds limiting their mobility. Altogether, the overall mobility of excitons is limited to a range of 10 nm, which is called the exciton diffusion length that is the distance over which an exciton can travel before decaying.

Exciton decay or charge carrier recombination can occur if excitons are generated too far from the interface. The BHJ concept of two intermixed materials decreases the diffusion length compared to a stacked bilayer structure and reduces the decay rate of excitons.

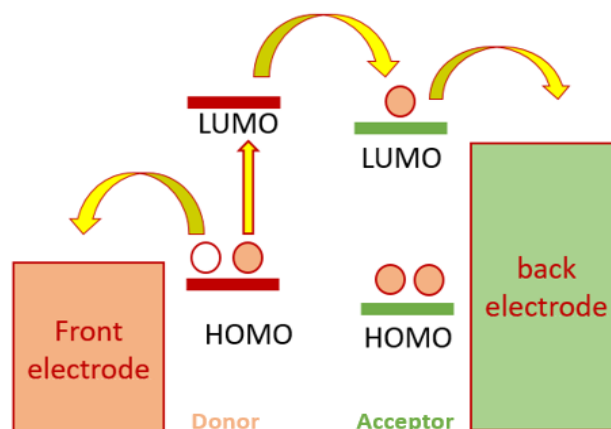


Figure 6. Working principle of organic solar cells.

2.3.3 Exciton dissociation (Charge separation)

Exciton undergo a charge transfer to the LUMO level of the acceptor as shown in Figure 7 where a charge-transfer (CT) state is created. Charges reside on different molecules but remain bound to each other by columbic attraction. Charges overcome this attraction and the CT state dissociates into two free charge carriers, an electron (negative charge carrier) and a hole (positive charge carrier). The dissociation of excitons occurs at donor:acceptor interfaces and is driven by an internal electric field caused by electrodes having different work functions. This exciton dissociation is driven by the difference between LUMO levels of the donor and that of the acceptor materials. For an efficient dissociation, the difference should be higher than that of the exciton binding energy. Typically, this difference is around 0.2 eV to 0.3 eV [32].

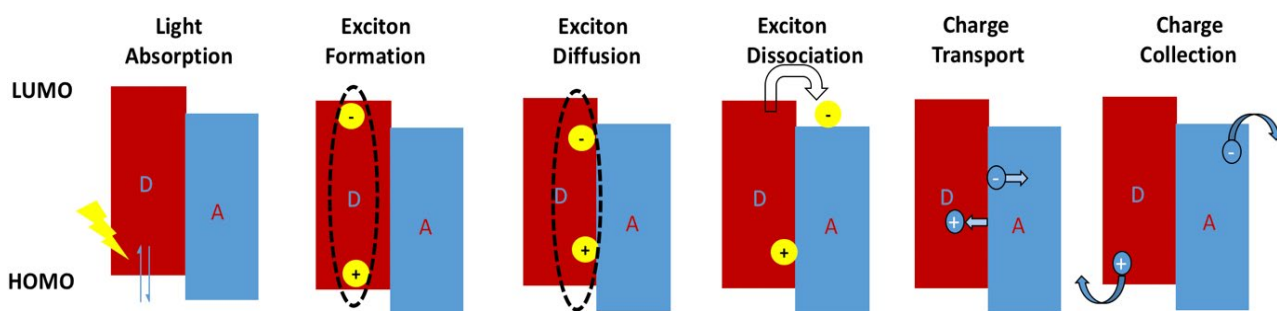


Figure 7. The fundamental steps for the working principle of an OSC.

2.3.4 Charge extraction and transport

The charge separation step produces individual charges, holes and electrons, that transport through neighboring p-type and n-type organic semiconductor domains, respectively, toward the corresponding electrode. The drift-direction of charge-carriers is influenced by the difference in work function of the two metallic contacts. The efficiency of charge transport is determined by electrical conductivity and impedance of organic materials.

2.3.5 Charge collection

After charge transportation, electrons are collected at the cathode electrode while holes are collected at the anode one. Photocurrent is generated by short circuiting or applying a voltage to an external circuit [33,34]. The 5 steps constituting the working principle of OSCs are illustrated in Figure 7.

3. State of art for OSCs

3.1 Optimizing the PCE of BHJ OPVs

For highly efficient BHJ OSCs, the following four critical factors shall be carefully considered: (1) light absorption, (2) energy levels, (3) charge mobilities and (4) morphology [35]. Based on these factors, several strategies were applied to increase the efficiency of OSCs. These include using low band gap polymers and non-fullerene acceptors, processing new device architectures and incorporating suitable interfacial layers.

3.1.1 New low band gap polymers

It has been found that the BHJ OPV constituted of polymer: fullerene blends are considered one of the most successful devices developed to date. For an efficient charge transfer, the minimum energy offset required between the LUMOs of polymers and LUMOs of fullerenes is about 0.3 eV. Therefore, the LUMO energy of an ideal donor should be approximately 3.9 eV (relative to 4.2 eV for PCBM LUMO). Additionally, to harvest solar photons effectively in donor polymers, the HOMO energy should reside at approximately 5.4 eV to ensure strong absorption at 700 nm [36]. Generally speaking, high band gap polymers as P3HT ($E_g = 2.1$ eV) cannot effectively harvest photons from the solar spectrum and are capable of absorbing only around 46% of the solar spectrum. Thus, lower bandgap polymers with an $E_g < 1.8$ eV are potential candidates for organic solar cells [37]. Normally, they possess higher absorption in the visible and near-IR region, matched energy levels with fullerenes, high carrier mobilities and excellent power conversion efficiencies thanks to the controlled intramolecular charge transfer from the donor to acceptor unit [38].

Poly[2,6-(4,4-bis-(2-ethylhexyl)-4H-cyclopenta[2,1-b;3,4-b]-dithiophene)-alt-4,7-(2,1,3-benzothiazole)] (PCPDTBT)[39] and poly[N-9'-hepta-decanyl-2,7-carbazole-alt-5,5-(4',7'-di-2-thienyl-2',1',3'-benzothiazole)] (PCDTBT) are low band gap polymers that can yield an efficiency up to 6.9% [40,41]. Other low band gap polymers were also investigated such as PTB7-Th (also known as

PCE-10) which is mainly crystalline [42] and the amorphous PTB7 [43]. The energy levels of these two polymers are more compatible with PC70BM fullerene than PC60BM. They exhibit good light responses, thus improving light absorption in the visible and near-infrared region. Solar cells based on PCE-10:PC70BM and PTB7:PC70BM blends were optimized leading to PCEs up to 9.34% and 8.18% at 0.27 cm², respectively, when processed under Argon [44].

Liu *et al.* [45] reported efficiencies up to 10.8% and fill factors (FF) up to 77% using three different donor polymers and several polymers:fullerene combinations. They focused on poly[(5,6-difluoro-2,1,3-benzothiadiazol-4,7-diyl)-alt-(3,3''-di(2-octyldodecyl)-2,2';5',2'';5'',2'''-quaterthiophen-5,5'''-diyl)](PffBT4T-2OD) that was combined with traditional PCBM (PC60BM and PC70BM) yielding 10.4% and 10.5%, respectively. When PffBT4T-2OD was blended with a non-traditional fullerene [6,6]-2-Thienyl-C70-butyric acid methyl ester (TC70BM), an efficiency of 10.8% was obtained. They claimed that the high polymer crystallinity and the excellent hole transport ability, combined with sufficiently pure polymer domains, are the main reasons beyond high efficiencies and FF. So far, BHJ OPVs based on polymer donors and fullerene derivative acceptors have shown the best performance with NREL-certified PCE of 11.5% using poly[(5,6-difluoro-2,1,3-benzothiadiazol-4,7-diyl)-alt-(3,3''-di(2-nonyltridecyl)-2,2';5',2'';5'',2'''-quaterthiophen-5,5'''-diyl)]PffBT4T-C9C13:PC70BM system [46].

Optimizing the active layer morphology (including crystallinity and miscibility of donor-acceptor), as well as enhancing fullerene derivatives' solubility were also used to improve device PCE [47].

3.1.2 Non-fullerene acceptors

Limitations of fullerene acceptors

Fullerenes and their derivatives have been found to be interesting materials as acceptor candidates in donor:acceptor blends owing to their high charge carrier mobility and electron affinity [48]. They can form favorable nanoscale phase separated domains in BHJs with suitable solvent additives [49]. Among all fullerenes, PC70BM is the most widely used acceptor for solution processed OPV devices. Although they have increased absorption in the visible region than PC60BM analogues, this absorption is believed to be weak preventing complementary light harvesting in acceptor domains. Furthermore, fullerenes have poor electronic tunability due to the limited number of different chemical structures that can be easily modified while still keeping C60 and C70 cores more or less intact. This will eventually limit donor:acceptor combinations [50,51].

Other limitations for fullerenes is their tendency to crystallize and form aggregates, which reduces the long-term stability of devices [52,53]. Additionally, fullerene-based solar cells cause large V_{oc} losses of 0.8 V to 1.3 V, which are much higher than those of other types of solar cells based on GaAs, silicon or perovskite (0.3 V to 0.5 V). These large losses are related to the non-sharp absorption edge of the BHJ, as well as the non-radiative losses that occur in most OPV systems [54,55]. Due to these challenges, the best reported PCEs are now near 10% to 12% which is the practical maximum efficiency limit predicted for polymer:fullerene bulk heterojunctions. Thus, in order to reach efficiencies between 15% to 20%, other approaches are required.

Using non-fullerene acceptors

In the case of single junction devices, the need for acceptors with higher absorption and energy tunability forced researchers to shift their efforts toward designing and studying alternative electron acceptors known as non-fullerene acceptors that could be either polymers or molecules [20]. NFAs possess several advantages when compared to fullerene acceptors. They can be easily synthesized with structural flexibility to match the frontier energy levels of donors, thus leading to efficient charge transfer. They have good solubility, planarity and crystallinity for better control of blend morphology and device stability. They are well known with their tunable bandgaps that improve light absorption in the near infrared region and tunable energy levels for achieving higher V_{oc} and lower energy losses [50,56]. After several optimization strategies including (1) structure design, (2) processing with additives and thermal annealing as well as (3) device configuration and others, the interest in such acceptors is growing. Numerous studies have been reported and the number of publications is rapidly increasing [35].

Single-junction OSCs based on NFAs achieved higher PCE than those of fullerene-based devices. An OSC based on a new polymer donor poly[(2,6-(4,8-bis(5-(2-ethylhexylthio)-4-fluorothiophen-2-yl)-benzo[1,2-*b*:4,5-*b'*]dithiophene))-*alt*-(5,5-(1',3'-di-2-thienyl-5',7'-bis(2-ethylhexyl)benzo[1',2'-*c*:4',5'-*c'*]dithiophene-4,8-dione))] (PBDB-T-SF which is known as PCE-13) and a new small molecule acceptor 3,9-bis(2-methylene-((3-(1,1-dicyanomethylene)-6,7-difluoro)-indanone))-5,5,11,11-tetrakis(4-hexylphenyl)-dithieno[2,3-*d*:2',3'-*d'*]-*s*-indaceno[1,2-*b*:5,6-*b'*]dithiophene (IT-4F) showed a record high PCE of 13.1% with an active area of 0.037 cm² [61]. Zhang *et al.* [62] showed that 3,9-bis(2-methylene-((3-(1,1-dicyanomethylene)-6,7-dichloro)-indanone))-5,5,11,11-tetrakis(4-hexylphenyl)-dithieno[2,3-*d*:2',3'-*d'*]-*s*-indaceno[1,2-*b*:5,6-*b'*]dithiophene (IT-4Cl) acceptor can deliver a PCE greater than 14% when combined with poly[(2,6-(4,8-bis(5-

(2-ethylhexyl-3-fluoro)thiophen-2-yl)-benzo[1,2-*b*:4,5-*b'*]dithiophen-*e*)-*alt*-(5,5-(1',3'-di-2-thienyl-5',7'-bis(2-ethylhexyl)benzo[1',2'-*c*:4',5'-*c'*]dithiophen-4,8-dione))] (PBDB-T-2F) with active area of 0.037 cm². The molecular structures and the absorption spectra of some ITIC derivatives and PCE-13 polymer are shown elsewhere [57,58]

Among the high efficiencies recorded were 16.5% and 15.3% with active areas of 0.09 cm² and 1 cm², respectively by blending the low bandgap NFA, 2,2'-((2*Z*,2'*Z*)-((12,13-bis(2-ethylhexyl)-3,9-diundecyl-12,13-dihydro-[1,2,5]thiadiazolo[3,4-*e*]thieno[2'',3'':4',5']thieno[2',3':4,5]pyrrolo[3,2-*g*]thieno[2',3':4,5]thieno[3,2-*b*]indole-2,10-diyl)bis(methanylylidene))bis(5,6-dichloro-3-oxo-2,3-dihydro-1H-indene-2,1-diylidene))dimalononitrile (BTP-4Cl) with poly[(2,6-(4,8-bis(5-(2-ethylhexyl-3-fluoro)thiophen-2-yl)-benzo[1,2-*b*:4,5-*b'*]dithiophene))-*alt*-(5,5-(1',3'-di-2-thienyl-5',7'-bis(2-ethylhexyl)benzo[1',2'-*c*:4',5'-*c'*]dithiophene-4,8-dione))] (PBDB-T-2F) polymer donor. Figure 8 shows the molecular structures of the used donor and acceptor molecules.

Recently, a record high PCE of 19.05% was realized for regular device structures by adding dithieno[3,2-*b*:2',3'-*d*]thiophene (DTT) additive into a ternary blend of poly[(thiophene)-*alt*-(6,7-difluoro-2-(2-hexyldecyloxy)quinoxaline)] (PTQ10) donor with fluorinated alkylthiophen-*e*-dithienothienopheno[3,2-*b*]-pyrrolobenzothiadiazole (BTP-FTh) and 2,2'-((2*Z*,2'*Z*)-((4,4,9,9-tetrahexyl-4,9-dihydro-*s*-indaceno[1,2-*b*:5,6-*b'*]dithiophene-2,7-diyl)bis(m-ethaneylylidene))bis(3-oxo-2,3-dihydro-1H-indene-2,1-diylidene))dimalononitrile (IDIC) NFAs. The chemical structures of the NFAs, PTQ10 donor, and DTT additive are shown in Figure 9.

As previously mentioned, the donor:acceptor combination is governed by the energy level compatibilities, that is the LUMO and the HOMO levels of both components. Figure 10 presents a schematic diagram of the energy levels of some donors and acceptors used for OSCs.

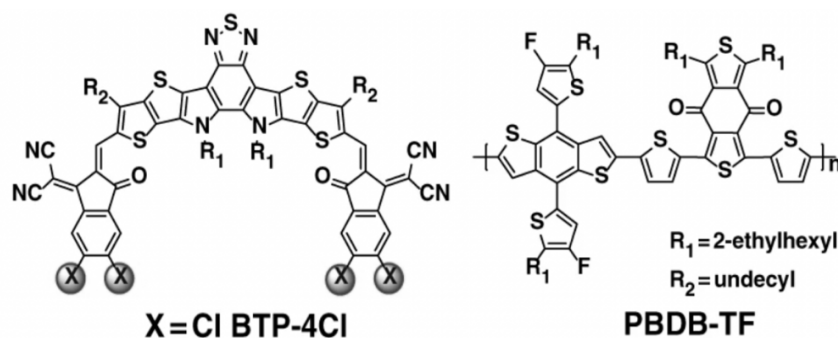


Figure 8. Chemical structures of BTP-4Cl acceptor and PBDB-T-2F donor.

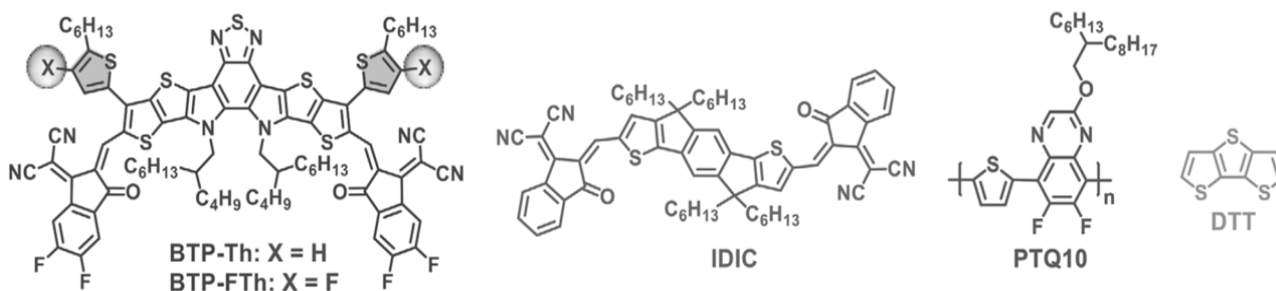
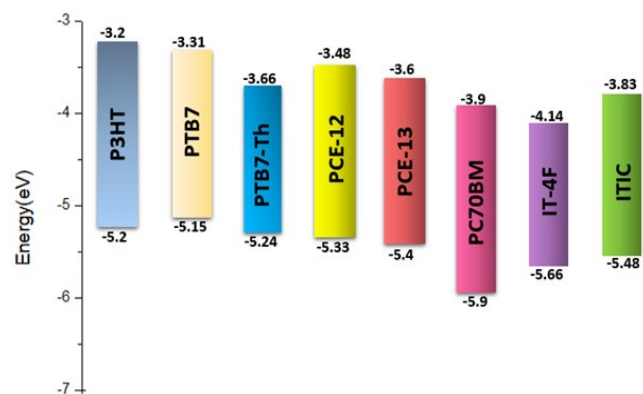


Figure 9. The chemical structures of the NFAs, PTQ10 donor, and DTT additive.

Table 1. Typical PV parameters of OSCs processed without HTL or with PEDOT:PSS and GQDs HTLs [61].

HTL	V _{oc} (V)	J _{sc} (mA·cm ⁻²)	FF (%)	PCE (%)
ITO only	0.46	10.54	47	2.28
PEDOT:PSS	0.93	11.4	65.3	6.92
GQDs (1.5 nm to 2 nm)	0.9	11.36	62.2	6.82

**Figure 10.** Schematic diagram of the energy levels of some donors and acceptors used for OSCs.

3.1.3 Suitable interfacial layers

Interfacial engineering has been identified as an essential approach for maximizing the power conversion efficiency of an organic solar cell. Metal oxides, polymers, small organic molecules, metals, metal salts/complexes, carbon-based materials, organic-inorganic hybrids/composites, and other emerging materials, are systemically used as electron and hole transporting materials for high performance OSCs. These interfacial materials with adequate WFs are desired to insert between the active layer and electrodes to match the energetic levels of donor and acceptor materials. This can enhance collection efficiencies of holes and electrons to the anode and cathode, respectively [59].

For example, by inserting an ETL of solution-processed ZnO nanoparticles (NPs) in a PTB7-Th:PC70BM-regular based device, the performance was greatly improved from 6.41% to 9.28% with an optimum ZnO layer thickness. This enhancement was due to the electron-extracting/hole-blocking properties of ZnO NPs in combination with a reduction of contact resistance and charge recombination at Al/BHJ interface.[60]

The same effect was detected in the presence of HTLs. Table 1 shows an efficiency of 2.28% for an OSC using a small molecule donor, 2,6-bis(trimethyltin)-4,8-bis(2-ethylhexoxy)benzo-[1,2-b:4,5-b'] dithiophene (DR₃TBTD) with PC70BM fullerene. This efficiency was increased to 6.92% and 6.82 % in the presence of PEDOT:PSS and graphene quantum dots (GQDs) HTLs, respectively [61].

4. Interfacial layers in organic solar cells

As previously mentioned, a typical device structure consists of a photoactive layer sandwiched between two charge-collecting electrodes. Thus, there are two kinds of interfaces that dominate such a device structure. The first interface is the donor/acceptor in which excitons are generated and dissociated into holes and electrons.

Another important interface is the organic/electrode interface. In theory, after exciton dissociation, holes and electrons will be collected at anode and cathode, respectively. This extraction is affected by the nature of the electrical contact between organics and electrodes [62].

In case of non-ohmic contacts, there is a mismatch of the electrode WF with the energy level of donor or acceptor materials causing a drop in V_{oc}. As an example, the WF of the commonly used cathode material, aluminium (Al), does not match the LUMO of the acceptor. Thus, inhibiting a good ohmic contact with the active layer [63]. In its turn, the ITO electrode cannot form as well an ohmic contact with the commonly used donor and acceptor materials in OSCs. This is due to the fact that its WF (4.8 eV), is not aligned neither with the HOMO level of most common donor polymers, nor with the LUMO of fullerenes [64].

To alleviate these interfacial energy barriers, proper interfacial materials have been employed as additional buffer layers between the BHJ layer and electrodes. This is considered as one of the essential approaches to maximize device PCE. They promote efficient extraction and transport of carriers and can suppress recombination between the active layer and the electrode. Thus, they can no more be considered as “optional” [13]. According to the type of the extracted charges, interfacial materials can be mainly classified into hole transport layers and electron transport layers.

We will begin this part with a summary of the general requirements that should be fulfilled by transport layers and then highlight on the detailed roles of these interfacial layers. A brief overview of the most commonly used HTLs in OSCs will be presented while pointing out the unique advantages of transition metal oxides interfacial layers.

4.1 Requirements for efficient ILs in OSCs

Efficient interfacial materials for OPV should fulfil several requirements with regard to their electronic, electrical, optical, chemical and mechanical properties.

They should promote good ohmic contact between the electrodes and the donor/acceptor materials of the active layer.

Good hole/electron transport properties (electrical conductivity) is required. Highly-conductive interlayers can help minimize resistance of devices and improve exciton dissociation [59]. Limited by low mobility, most of the organic based interlayers employed so far in devices and some metal oxide layers have been restricted to few nanometers in thickness. To solve this issue, doping organic interfacial materials has been applied to improve their electrical conductivities. As an example, the conductivity of the electron-transporting semiconductor bathocuproine (BCP) can be enhanced by several orders of magnitude after being doped with Ytterbium (Yb) [65]. Not only organic materials can be doped but also metal oxide interfacial layers can have enhanced conductivities by doping such as in the case of Al doped ZnO ETL [66].

They must possess appropriate ionization potential and electron affinity values to enhance the selectivity of holes and electrons toward the anode and cathode, respectively.

Transparency is required in both regular and inverted device structures for HTL and ETL, respectively to minimize optical losses by absorption [13,67].

They should be producible at low cost.

They need to have chemical and physical stability to prevent undesirable reactions at the active layer/electrode interface.

They must be mechanically robust to support multilayer solution processing [68].

4.2 Roles of interfacial layers in OSCs

In this part, the roles and importance of interfacial materials introduced in OSCs will be discussed in details.

4.2.1 Tuning energy level at the organic/electrode interface

Having a proper energy level alignment at the organic/electrode interface has been proven to enhance charge collection efficiency and V_{OC} of devices [69]. To achieve maximum V_{OC} , Ohmic contact with electrodes is required, since Schottky barrier (non-ohmic contact) formed at either electrodes will create potential loss with undesirable charge accumulation. This will lower the resultant V_{OC} and decrease device efficiency [64]. To address this issue, interfacial materials are applied to pin the electrodes' Fermi-levels to the photo-excited quasi-Fermi level (E_F) of organic semiconductors (acceptor, E_{F,e^-} , and donor, E_{F,h^+}) under illumination [70,71].

4.2.2 Improving charge transport and electrode selectivity

A suitable buffer layer does not only adjust the energetic barrier height between the active layer and electrodes, but also increases the selectivity of the corresponding electrode for holes and electrons. Thus, preventing unfavorable charge recombination or exciton quenching at the organic/electrode interfaces and improving device FF. For an ideal HTL, the HOMO level should align with the E_{F,h^+} of the BHJ layer while its LUMO level should be located above the E_{F,e^-} of the BHJ layer. In such a way, it can only collect holes while blocks electrons. The same principle should be applied to the ideal ETL to collect electrons and block holes [68].

4.2.3 Determining devices' polarity

The bottom electrode is the transparent electrode, *e.g.* ITO, on which the OPV cell is constructed. In an ideal case, the donor and acceptor materials are distributed equally throughout the blend of the active layer. Thus, the preferential direction to extract electrons or holes to one side of the solar cell is not determined by the active layer but dependent on the type of the interfacial layer placed on top of the bottom electrode. Fortunately, the WF of ITO can be modulated by surface modification. Depending on the nature of the modification material, ITO can be used as anode or cathode when modified with high or low WF buffer layers, respectively [72]. For instance, PEDOT:PSS is commonly used to improve ITO's hole extraction, while ZnO

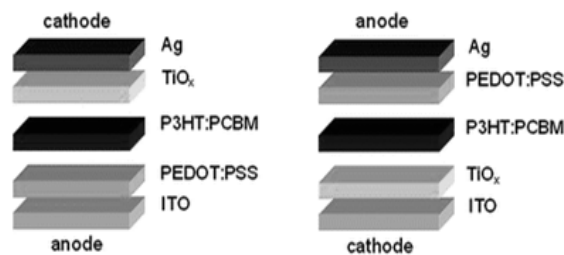


Figure 11. An OSC in the regular (left) and inverted device structure (right).

or TiO_x are used to enhance its electron extraction (Figure 11). In some cases, even stable metals such as Ag can be used as cathode when appropriate interfacial materials are applied.

4.2.4 Optical spacer effect

Most OPV devices consist of a transparent front electrode and a non-transparent reflecting back electrode. Light enters the OPV cell through the transparent electrode where it is absorbed by the photoactive layer and reflected at the non-transparent electrode. The thickness of the organic BHJ layer is generally restricted to 100 nm to 200 nm to avoid severe charge recombination caused by the low carrier mobility and short exciton diffusion lengths of the absorbers. Such thin film will suffer from optical transmission dissipation and insufficient light absorption, thereby decreasing short-circuit current density (J_{SC}) [73,59]. In this regard, optical spacer effect is a concept used to enhance light absorption of photoactive layers by inserting a transparent interfacial layer between the reflecting electrode and the active layer. Depending on the refractive index and the thickness of the introduced layer, the absorption maximum can be shifted into the photoactive layer.

An example of an OPV cell with and without optical spacer is shown in reference [72]. It constitutes of ITO/PEDOT:PSS/P3HT:PC60BM/ TiO_x /Al where TiO_x acts as an optical spacer. Another example is ZnO optical spacer in PTB7:PC70BM-based regular devices. In this case, ZnO improves light absorption in the bulk at a specific thickness and enhances all the photovoltaic parameters, not only J_{SC} [74].

4.2.5 Protective layer between the polymer and the electrode

One of the important roles of an IL is protecting the organic layer from physical or chemical interaction with electrodes [72]. Metals are often used as electrode materials, however, diffusion of metal atoms into polymeric layers during thermal evaporation process causes electrical shorting of the organic devices and limits their lifetime [75]. Thus, the presence of an IL can protect the photoactive layer from this metal diffusion. Interfacial layers can also serve as "protectors" against ITO roughness as in the case of PEDOT:PSS [76].

4.2.6 Enhancing device stability

Besides efficiency, stability is another important aspect to be improved to make OPV a competitive solar technology. The photoactive layer is susceptible to chemical degradation, especially under illumination in the presence of oxygen and water. Encapsulation is considered

as a solution to slow down degradation processes by preventing oxygen and water diffusion into the device. However, the development of more stable devices is still much important. This property has been demonstrated by the incorporation of interfacial layers. For example, TiO_x can act as oxygen and water scavengers to enhance air stability of organic solar cells [77]. Recently, it has been demonstrated that the instability of non-fullerene acceptor solar cells primarily arises from chemical changes at the organic/inorganic interfaces and that a careful treatment of these interfaces could incredibly enhance device stability [8].

4.3 Materials for hole transport layers in OSCs

A hole transport layer is also known as hole extraction layer (HEL) or anode buffer layer. The main role of this HTL is to improve collection and extraction efficiency of holes. Since ITO with its WF cannot form an ohmic contact with the used donors, hole transport materials with high WFs are needed to match the HOMO levels of donors in the active layer and facilitate hole extraction. To date, many HTLs have been designed for both regular and inverted device structures. The most commonly used ones include:

4.3.1 Graphene oxide (GO)

The high WF GO (4.9 eV to 5.1 eV) is an efficient HTL for OPVs. GO is a graphene sheet functionalized with oxygen functional groups in the form of epoxy and hydroxyl groups prepared by chemical oxidation. Its solution processability and unique electrical and optical properties endow it as a promising nanomaterial for various applications. The bandgap of GO was reported to be 3.6 eV, while its HOMO and LUMO levels are -5.2 eV and -1.6 eV, respectively. These energy levels suggest that GO can transport holes and block electrons, making it a potential good hole selective material for OPVs [78]. Incorporating GO hole transport layer into a PCDTBT:PC70BM-based organic photovoltaic solar cell increased the efficiency from 2.7% up to 5.1%. This PCE was comparable to that using PEDOT:PSS HTL (5.3%). The J-V curves of the different fabricated devices with a large active area (0.64 cm^2) were reported [79].

Layer-by-layer (LbL) assembled GO thin films were used as HTLs in devices based on P3HT:I60CBA ([5,6] fullerene- C_{60}) active layers. Without any HTL, the device showed a poor efficiency of 2.97%. By inserting GO layers with an optimized number of deposition times (n), the WF of ITO was improved leading to a better contact with the active layer. Therefore, the PCE of the OSC was increased to 6.04% with GO-2 which was comparable to that based on PEDOT:PSS HTL.[80] These comparable efficiencies were due to the fact that WFs of all GO films were in the range of 4.9 eV to 5.0 eV, which was close to that of PEDOT:PSS (5.0 eV). The reason beyond the increased work function of GO (from 4.7 eV to 5 eV) was the ultraviolet-ozone (UVO) treatment.

Despite its role as an efficient transport layer, GO suffers from its insulating nature which limits the layer thickness to 2 nm when used in devices. In this regard, various chemical or thermal reduction strategies were applied to convert GO back to its pristine conjugated structure, thus enhancing its electrical conductivity. Such reduced GO (r-GO) is considered to have better charge extraction ability compared

to GO [81]. One example is the incorporation of a UV-ozone treated GO/PEDOT:PSS bilayer functioning as a HTL in PCDTBT:PC70BM-based devices. In such devices, the HTL was treated with UVO for 0, 5, 10 and 15 min, in which the 10 min-treated bilayer lead to the best performance of 5.24%. This improvement was attributed to both, reduction of GO and increased WF of PEDOT:PSS after UVO treatment. This induces better contact conditions with the photoactive layer, enhancement in hole extraction and decreasing in the probability of recombination. The time for UVO exposure should be optimized to get the best effect. Exposing the layer for a longer time caused severe reduction in the PCE to 2.11%, possibly due to various factors such as decomposition of chemical bonds or increase in series resistance (R_s) [82].

4.3.2 PEDOT: PSS

PEDOT:PSS is the widely used HTL in OSCs.[59] Usually PEDOT is doped with PSS for an improved conductivity and solubility in protic solvents. One of the advantages of PEDOT:PSS is that a wide range of electrical conductivities from $10^{-6} \text{ S}\cdot\text{cm}^{-1}$ to $10^3 \text{ S}\cdot\text{cm}^{-1}$ can be achieved by changing the compositional ratio between PEDOT⁺ and its PSS⁻ [68]. The chemical structure of PEDOT:PSS is shown in Figure 12.

PEDOT:PSS is an easy solution processed material with a high work function reported between 4.8 eV and 5.2 eV. This allows the formation of an Ohmic contact with the HOMO level of most common donor polymers [13]. It has a good optical transparency (higher than 80%) over the visible-near IR range which minimizes absorption losses. Interestingly, PEDOT:PSS is able to reduce ITO surface roughness, while increasing its work function [67]. Some of the best reported OPV efficiencies are those using PEDOT:PSS HTLs. In regular PTB7-Th:PC70BM and PTB7:PC70BM-based devices, PCEs of 9.34% and 8.18% were achieved, respectively, using PEDOT:PSS as HTL and ZnO as ETL [44]. By replacing ZnO with a non-conjugated small molecule named 4,4'-(((methyl(4-sulphonatobutyl)ammonio)bis-(propane-3,1-diyl))bis(di methyl-ammoniumdiyl)) bis-(butane-1-sulphonate) (MSAPBS), a PCE of 10% was achieved for PTB7:PC70BM-based devices [83]. Another regular device structure with PEDOT:PSS -HTL and Ba ETL showed around 8.57% with a small molecule donor [84].

Using zirconium acetylacetonate (ZrAcac) ETL, the PCE of devices based on PBDTTT-C-T:PC70BM reached 7.55% when PEDOT:PSS HTL was employed [85]. An 8.52% efficiency was achieved with PCE-12:PC60BM-based devices using cesium oxide (CsO_x) and PEDOT:PSS ETL and HTL, respectively [86].

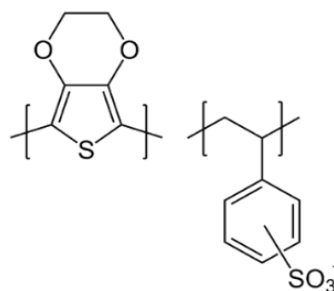


Figure 12. The chemical structure of PEDOT:PSS.

Hybrid inorganic/organic solution-processed HTLs employing molybdenum oxide (MoO₃)/PEDOT:PSS composite materials were developed, taking advantage of both the highly conductive PEDOT:PSS and the ambient condition stability of MoO₃. The resulting bulk heterojunction OSCs based on TQ1:PC70BM showed considerable improvement in PCE from 5.5% to 6.4%, compared to the reference pristine PEDOT:PSS-based devices. More importantly, devices with MoO₃-PEDOT:PSS HTLs showed a considerable improve in stability, in which the efficiency retained 80% of its original value when the devices were stored in ambient air and dark for 10 days. In comparison, reference solar cells using PEDOT:PSS HTLs showed complete failure within 10 days [87].

Blending BTP-eC9 NFA with PBDS-T donor for a regular device structure using PEDOT:PSS HTL resulted in a device PCE of 16.4% with the help of a low refractive index antireflection layer (MgF₂) [88].

Interestingly, record high efficiencies were obtained using PEDOT:PSS HTLs for regular device structures employing ternary blends of one donor and two NFAs. For example, a maximum PCE of 19.0% (certified value of 18.7%) was achieved for a PBQx-TF:BTP-eC9-2Cl:F-BTA3 blend. The improved light unitization, cascaded energy level alignment, and enhanced intermolecular packing result in a V_{OC} of 0.879 V, J_{SC} of 26.7 mA·cm⁻², and FF of 0.809. The resulting binary cell exhibits as well a good PCE of 17.7% [89].

Another record high PCE of 19.05% was obtained using a PTQ10:BTP-FTh:IDIC blend based on a regular structure of ITO/PEDOT:PSS/active layer/PNDIT-F3N/Ag [6]. The detailed PV parameters of the fabricated OSCs using different blend and DTT additive ratios are summarized in Table 2.

Despite the high efficiencies obtained using PEDOT:PSS HTL in regular device structures, some authors stated that PEDOT:PSS has limited electron blocking properties, as compared to other kinds of materials [13]. Also, its extreme acidic (pH 1-2) and hygroscopic nature cause ITO corrosion and influence the stability of OSCs which necessitates its replacement with other solution processed hole transport materials [90]. Moreover, its high hydrophilicity is considered a serious obstacle for inverted device structures. Bad film morphology and worse electrical properties have been observed when PEDOT:PSS was deposited onto hydrophobic organic layers. The wettability problems on hydrophobic surfaces can be solved by adding proper additives capable of reducing the hydrophilic nature of PEDOT:PSS such as Triton X-100.[91] Using modified PEDOT:PSS HTLs in P3HT:IC60BA [92] and P3HT:PC60BM-based inverted device structures, [91,93] efficiencies of 6.2% and 4% were obtained, respectively. Due to the limited PCEs in inverted device structures, it is highly recommended to replace such modified layers with alcoholic-based HTLs.

Table 2. Photovoltaic parameters of the OSCs based on a PTQ10 donor.

Acceptor	DTT (wt%)	V _{oc} (V)	J _{sc} (mA·cm ⁻²)	J _{EQE} ^{a)} (mA·cm ⁻²)	FF (%)	PCE ^{b)} (%)
BTP-FTh:IDIC (0.9:0.1)	0	0.859	26.56	25.92	77.9	17.77 (17.34 ± 0.37)
BTP-FTh:IDIC (0.8:0.2)	0	0.867	26.97	26.23	78.6	18.39 (18.01 ± 0.35)
BTP-FTh:IDIC (0.7:0.3)	0	0.872	26.74	26.05	75.7	17.65 (17.08 ± 0.35)
BTP-FTh:IDIC (0.8:0.2)	10	0.870	27.17	26.64	80.6	19.05 (18.68 ± 0.33)
BTP-FTh:IDIC (0.8:0.2)	20	0.862	25.70	25.05	76.0	16.84 (16.39 ± 0.37)

4.3.3 Transition metal oxides

Transition metal oxides (TMOs) are promising candidates to replace PEDOT:PSS because of their better environmental stability, higher optical transparency, easier synthetic routes and superior electronic properties [94]. They possess high WF and large energy band gap ($E_g > 3$ eV) [90]. In general, TMOs can be classified into n-type and p-type semiconductors according to their corresponding electronic states and intrinsic point defects, such as atomic vacancies (oxygen vacancies) present in oxides. Ultraviolet Photoelectron Spectroscopy (UPS) and Inverse Photoemission Spectroscopy (IPES) are widely used techniques for the measurement of valence band (VB) and conduction band (CB) states. Molybdenum oxide (MoO₃), vanadium oxide (V₂O₅) and tungsten oxide (WO₃) possess very deep lying electronic states, with a VB edge around 2.5 eV to 3 eV below the Fermi level and a CB edge very close to the Fermi level. These are indicative of highly n-type materials. Accordingly, when used as HTLs, the Fermi-level pinning between the photoactive layer and TMOs can be achieved by matching the CB of TMOs and the HOMO level of the donor in the BHJ. The VB edge of these TMOs is derived from the occupied O 2p orbital while the CB is derived from the unoccupied transition metal d orbital. Fully stoichiometric MoO₃, V₂O₅ and WO₃ are known to be insulators. However, the n-type conductivity of these oxides is most likely a result of a slightly non-stoichiometric composition, with some oxygen deficiencies [95].

Differently, p-type TMOs like nickel oxide (NiO_x) with slightly lower WF than the n-type ones have a Fermi level close to the VB edge. They accomplish the Fermi-level pinning with the HOMO level of the donor through their VB level. It is well known that pure stoichiometric nickel oxide is an excellent insulator with conductivity of 10⁻¹³ S·cm⁻¹, while non-stoichiometric NiO_x is a wide-bandgap p-type semiconductor with conductivities of ≈10⁻³ S·cm⁻¹ to 10⁻⁴ S·cm⁻¹. Unlike all n-type oxides in which their semi-conductivity stems from the negative charge compensation at defect sites of oxygen vacancies and/or cation interstitials, the p-type characteristics of NiO_x originate from the positive charge compensation which favored Ni²⁺vacancies. Since the VB of NiO_x is between 5.0 eV to 5.4 eV and the CB is around 1.8 eV, which is higher than the LUMO level of the donor, NiO_x can efficiently collect holes from the donor phase (selective to holes) and is effective in blocking electrons. In contrast, the energy levels (low CB edge) of the n-type anode buffer materials (WO_x, MoO_x, and VO_x) indicate that they do not possess electron-blocking properties.[95]

The exact classification of TMOs into n-type and p-type is illustrated in Figure 13.

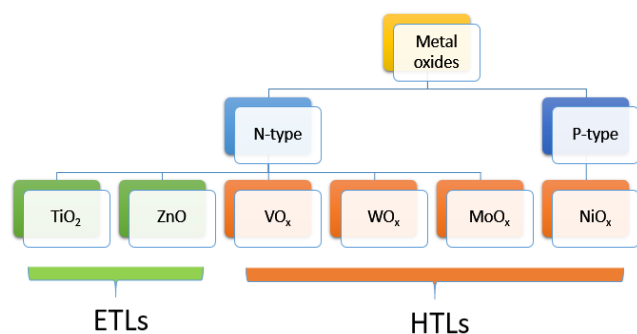


Figure 13. Classification of TMOs into n-type and p-type.

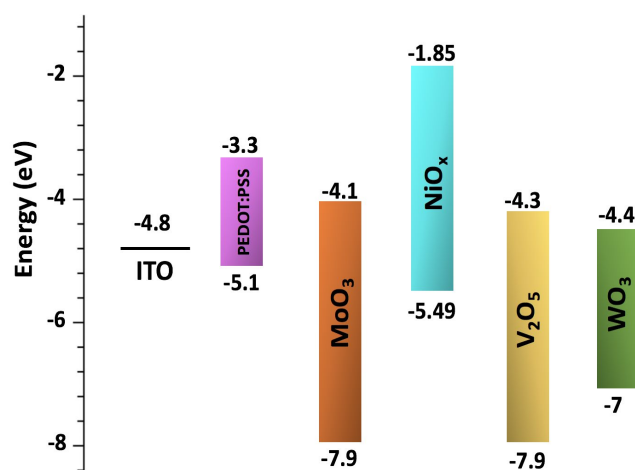


Figure 14. Schematic energy level diagram of typical HTLs used for OSCs.

For the preparation of TMOs HTL, one can differentiate between two approaches. The physical approaches including thermal evaporation, sputtering, atomic layer deposition, pulsed laser deposition and others are highly expensive and require harsh conditions. This will limit their use for large area device fabrications. As an alternative, some research groups have developed solution processing methods for the deposition of metal oxide films. In turn, these solution-processed synthetic methods can be classified into precursor and nanocrystals approaches. The so-called precursor approach is based on depositing soluble metal precursors onto substrates, followed by in situ reactions, such as sol-gel hydrolysis or combustion reactions. Normally, high temperature annealing is required to induce decomposition and crystallization. This will limit its application to the bottom interfacial layers and make this precursor solution impossible to be processed on top of active layers or flexible substrates. Thus, the alternative colloidal nanocrystal approach is favored. The main advantage of this approach is decoupling the crystallization of oxides from film-formation process. Thus, providing more freedom on the synthesis of oxide materials. Using this method, harsh reaction conditions e.g. high pressure and high temperature can be applied, and many purification methods such as extraction or recrystallization can be utilized to purify the products. Interestingly, the nanocrystal approach makes the deposition of oxide-nanocrystal interfacial layers possible to be processed at low temperature, unlike the precursor approach [96].

Chemical precipitation, solvothermal and hydrothermal processes are examples of nanocrystal approaches.

It is worth mentioning that the WF of all TMOs is strongly correlated with their synthetic methods, way of deposition, surface characteristics, and crystal structures [59]. Figure 14 illustrates the energy level diagram of typical HTLs used for OSCs.

4.3.3.1 Vanadium oxide

Vanadium oxide (V_2O_5 or VO_x) is actually n-type semiconductor used as efficient HTL for both regular and inverted device structures, but it is well known for its high toxicity.[97] V_2O_5 films can be either thermally evaporated or solution processed with WF of 7 eV and 5.3 eV, respectively, thus, providing an excellent Ohmic contact to organic materials with large HOMO energies [90].

Solution-processed V_2O_5 buffer layers were prepared by spin coating vanadium(V) tri-isopropoxide from isopropyl alcohol solution on ITO electrodes. These layers were subsequently stored at ambient air/1 hour for hydrolysis without any post treatment. It was demonstrated that these sol-gel derived V_2O_5 layers can replace PEDOT:PSS HTLs in OSCs. Consequently, P3HT:PC60BM-regular based devices with 10 nm thick V_2O_5 HTLs showed comparable or even better photovoltaic characteristics than devices fabricated with PEDOT:PSS HTLs. The efficiencies were 3% and 2.7%, respectively. What is worth mentioning is that V_2O_5 -based cells retained 80% of their initial efficiency after being exposed to air for 400 h while PEDOT:PSS-containing cells were completely degraded [98].

By using poly({4,4,9,9-tetrakis(4'-hexylphenyl)-2-thiophen-2-yl-benzo[1'',2'':4,5; 4'',5'':3',4']dicyclopenta[1,2-b:1',2'-b']dithiophene} {5,7'-(4'-2-thienyl-2',1',3'-benzothiadiazole)}) (PTPTBT) donor and PC70BM acceptor, higher efficiency was reached with V_2O_5 buffer layers (5%) in comparison to devices based on PEDOT:PSS buffer layers (3.6%) [99]. In its turn, PBDTTT-C:PC70BM-regular based device using V_2O_5 HTL showed a higher PCE of 7.54% when compared to those devices based on PEDOT:PSS (6.52%) or thermally evaporated V_2O_5 (6.27%) [100].

The same sol-gel derived vanadium oxide can be used for inverted device structures. In this regard, the performance of P3HT:PC60BM-inverted based devices with evaporated V_2O_5 HTL was compared to that with sol-gel-processed V_2O_5 HTL. The thermally evaporated 20 nm thick V_2O_5 layer resulted in a device efficiency of 2.9% which was quite comparable to the 3% efficiency achieved by the 10 nm thick solution processed V_2O_5 layer [101]. Vanadyl acetylacetonate $VO(acac)_2$ is another precursor that can be spin coated from isopropanol solution to prepare VO_x buffer layers, followed by thermal annealing at 150°C for 10 minutes. The power conversion efficiency of the resulting regular device structures based on P3HT:IC70BA reached 6.35% [102].

Vanadium oxide layers were also prepared by oxidizing the vanadium powder using hydrogen peroxide to obtain hydrogen vanadium oxide bronzes that can be dispersed in ethanol. With mild temperature treatment not greater than 100°C, the obtained TMO films with small amount of oxygen vacancies exhibited high film quality and desirable electrical properties showing 7.62% efficiency in PBDTTT-C-T:PC70BM-regular based device structures [103].

Table 3. The photovoltaic parameters of P3HT:PC60BM-based OSCs using various HTLs.

HTL	V _{oc} (V)	J _{sc} (mA·cm ⁻²)	PCE (%)	FF (%)
PEDOT:PSS	0.60 (0.60 ± 0.005)	9.83 (9.81 ± 0.23)	3.58 (3.53 ± 0.07)	60.52 (60.28 ± 1.26)
SC-V ₂ O ₅	0.59 (0.59 ± 0.006)	9.67 (9.63 ± 0.23)	3.78 (3.74 ± 0.12)	66.69 (66.27 ± 0.59)
BP-V ₂ O ₅ at 50°C	0.59 (0.59 ± 0.001)	9.77 (9.77 ± 0.07)	3.83 (3.82 ± 0.01)	66.71 (66.47 ± 0.47)

Another interesting approach was demonstrated by Choy *et al.* [104] showing the possibility to fabricate an organic solar cell using the same metal oxide for both ETL and HTL. This was made possible by the adjustment and control of work function. For example, the WF of V₂O₅ was shifted from 5.43 eV to 4.15 eV by cesium (Cs) intercalation making Cs-V₂O₅ more n-type semiconductor, which offers better electron transport properties. Thus, inverted device structures constituting of ITO/Cs_xV₂O₅/PBDDTTT-S-T:PC70BM/V₂O₅/Ag yielded an efficiency of 6.08%.

Other than spin coating, V₂O₅ can be deposited by brush painting method on top of the electrode without any post treatments yielding an efficiency of 3.83% [105]. The photovoltaic parameters of P3HT:PC60BM-based OSCs are summarized in Table 3.

4.3.3.2 Tungsten oxide

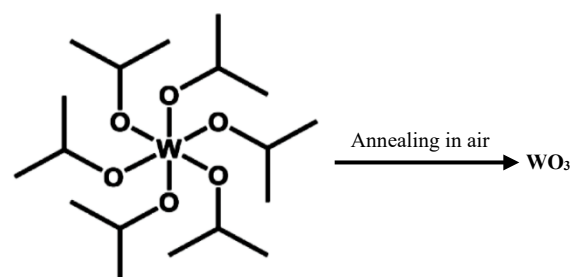
Tungsten oxide (WO₃) is another n-type metal oxide with high WF, which can promote good ohmic contacts with many polymer donor materials used in OSCs. The WF of the freshly evaporated WO₃ is around 6.05 eV with an optical band gap between 3.25 eV and 3.41 eV. This WF is sensitive to oxygen deficiency and exposure; it can decrease to 4.7 eV upon oxygen exposure. On the other hand, the WF of solution processed WO₃ is 5.15 eV. Thus, the electronic structure highly depends on stoichiometry, crystalline structure and deposition conditions [94,106]

P3HT:PC60BM-inverted based devices using evaporated WO₃ as top anode interlayers and solution processed TiO_x as bottom cathode interlayers were reported by Tao *et al.* [107] in which they displayed an efficiency of 2.58%. Whereas, in the case of regular P3HT:PC60BM-based devices, the performance was a bit higher reaching 3.1% [108].

Regarding solution processed WO₃ layers, tungsten alkoxides, such as tungsten ethoxide (W(OC₂H₅)₃ or W(OC₂H₅)₆) and tungsten(VI) isopropoxide (W[OCH(CH₃)₂]₆), were used as precursors to prepare WO₃ anode buffer layers. Tan *et al.* [109] prepared WO₃ HTLs through sol gel process by spin coating tungsten(VI) isopropoxide solution, followed by thermal annealing at 150°C for 10 min in air. This treatment results in complete decomposition of the precursor into WO₃. This transformation is shown in Figure 15.

Regular P3HT:IC70BA-based devices with solution processed WO₃ HTLs showed enhanced performance (6.36%) in comparison with devices incorporating PEDOT:PSS HTLs [109].

Another sol-gel process utilizing tungsten ethoxide [W(OC₂H₅)₆] was studied where the precursor was spin coated on top of ITO substrates and films were stored in air overnight to complete hydrolysis and condensation reactions. The WO₃ layer thickness was controlled based on the concentration of the prepared precursor. After optimizing the thickness to 10 nm and incorporating it in a device of the following structure: ITO/WO₃/P3HT:PC60BM/Al, the obtained PCE (3.4%) was

**Figure 15.** Transformation of tungsten(VI) isopropoxide into WO₃

comparable to those devices utilizing PEDOT:PSS HTLs. However, PCEs were decreased to 40% and 0% of their initial values, when PEDOT:PSS-based devices were exposed to air and light for 192 h, respectively. However, PCEs maintained 90% and 87% of their initial values, respectively, when WO₃-based devices were exposed to the same conditions. Thus, tungsten oxide buffer layers can afford a much higher stability than PEDOT:PSS layers due to their air and photo-stability [110].

A low-temperature (80°C)-processed WO₃ HTL has been developed by Brabec *et al.* [111] without oxygen post-treatment. It works well for both regular and inverted device structures giving 2.4% for inverted P3HT:PC60BM-based devices and 3% for regular devices in comparison with 3.2% for PEDOT:PSS-based regular device structures. By changing the active layer of the inverted device to Si-PCPDTBT:PC70BM, 4.8% and 5% were achieved with WO₃ and PEDOT:PSS HTLs, respectively. It is worth mentioning that the deposition method used was doctor blading and not spin coating.

Kwon *et al.* [112] compared the performances of MoO₃ and WO₃-based inverted devices using PTB7:PC70BM active layers. By incorporating 10 nm-thick MoO₃ HTL, the PCE obtained was 6.48%. However, by replacing MoO₃ with a 5 nm-thick WO₃ layer, the efficiency was slightly better (6.67%). Kwon *et al.* explained the better behavior of WO₃ layer with: (1) better film surface morphology, thus a reduced average roughness, (2) better measured conductivity and (3) better electron blocking and hole transporting properties. This is due to the higher energy barrier between the donor LUMO and the HTL conduction band and the better energy matching between the donor HOMO level and the valence band of the HTL.

Based on previous studies, the morphology of BHJ films critically depends on the surface free energy (γ_s) of the underlying interfacial layer. Therefore, to attain satisfactory device behaviors, the γ_s of the underlying interfacial layer should be carefully modified to adapt to the chemical structure of BHJ materials without sacrificing charge extraction properties and morphology of the BHJ. Concerning the higher γ_s of metal oxide nanoparticles than conjugated polymeric films, some metal oxides have been taken into consideration to modify the γ_s of PEDOT:PSS. Based on this fact, WO_x NPs were suitable

candidates as PEDOT:PSS modifiers since they display an adaptive WF to a wide range of BHJ layers. Additionally, they have good dispersion in polar solvents and high stability in acids. Thus, a strategy incorporating WO_x nanoparticles into PEDOT:PSS was utilized to form a hybrid WO_x :PEDOT:PSS composite HTL with an improved surface free energy that optimizes the morphology of the active layer. This hybrid interfacial layer was applied into fullerene-free organic solar cells based on PBDB-T-2F:IT-4F blend and PFN-Br ETLs. A high PCE of 14.57% with FF approaching 81% was achieved by optimizing different parameters. The results were certified by the National Institute of Metrology (NIM). On the other hand, devices incorporating PEDOT:PSS or WO_x gave 13.29% and 8.73%, respectively [113].

4.3.3.3 Molybdenum oxide

Molybdenum oxide (MoO_3 or MoO_x) is an excellent hole transport material and was once misidentified as a p-type semiconductor until n-type characteristics were directly determined by UPS. Molybdenum oxide can be deposited by thermal evaporation with a thickness control at a nanometer scale. The evaporated MoO_3 (e- MoO_3) forms an Ohmic contact with many organic hole transporting materials by having a work function around 6.5 eV to 6.9 eV. Solution processed MoO_3 materials were also utilized as HTLs having a lower work function of 5.3 eV to 6 eV. Further studies revealed that the work function is dependent on the stoichiometry of molybdenum oxide and is highly sensitive to surface contaminations [90,94]

e- MoO_3 were used in regular device structures based on PCDTBT:PC70BM active layers giving an efficiency of 6.5% which was higher than that of PEDOT:PSS-based devices (5.95%) [114]. Table 4 summarizes the photovoltaic parameters of this device system using either PEDOT:PSS or e- MoO_3 layers of several thicknesses.

e- MoO_3 HTLs were also applicable in inverted device structures based on PDTG-TPD:PC70BM and PDTS-TPD:PC70BM systems [115] in which the PCEs obtained exceeded 8% and 7.8%, respectively (Table 5).

Interestingly, fabricating an inverted device structure with a chlorinated non-fullerene acceptor (BTP-4Cl) and PBDB-T-2F polymer achieved record PCEs of 16.5% and 15.3% for cells having 0.09 cm² and 1 cm² active areas, respectively [19]. Recently, inverted device structure using encapsulated devices stabilized by additional protective buffer layers (a self-assembled monolayer on the ZnO ETL together with fullerenes before the e- MoO_3 HTL) as well as the integration of a simple solution processed ultraviolet filtering layer, could lead to amazing stability, with intrinsic lifetime equivalent to 30 years of outdoor exposure [8].

Regarding solution processed MoO_3 , a facile method has been introduced by Yang *et al.* [116] to prepare low-temperature processed MoO_3 HTLs. This method was based on thermal decomposition of ammonium heptamolybdate precursor $(NH_4)_6Mo_7O_{24} \cdot 4H_2O$ into three components, MoO_3 , NH_3 and H_2O . Among these components, NH_3 will be evaporated into air and MoO_3 was expected to be the only solute in the solution. The prepared solution was spin coated on top of ITO substrates that were then annealed at 100°C for 10 min in air to examine their efficiency with regular P3HT:PC60BM-based devices. A PCE of 3.74% was obtained which was comparable to

that recorded using PEDOT:PSS HTL (PCE = 3.77%) but higher than that using thermally evaporated MoO_3 (PCE = 2.77%). The performances of devices show that the optimum concentration for MoO_3 was 0.2 wt%.

Chou *et al.* [103] proposed a one-step method to synthesize low temperature solution-processed molybdenum oxide. These HTLs were used to fabricate high performance regular PBDTTT-C-T:PC70BM-based devices having 7.75% efficiency, which were outperforming the control PEDOT:PSS-based device. The MoO_3 buffer layers were obtained by spin coating a solution of hydrogen molybdenum bronze resulted from the oxidation of molybdenum powders by hydrogen peroxide. With a mild temperature treatment not greater than 100°C, the obtained TMO films with small amount of oxygen vacancies exhibited high film quality and desirable electrical properties.

Sol-gel processed MoO_x was also reported in which molybdenum diacetylacetonate dioxide ($MoO_2(acac)_2$) precursor was spin coated on ITO substrates, that were then baked in air at 150°C for 10 min to be completely transformed into MoO_x . The power conversion efficiency of regular P3HT:IC70BA-based devices using these MoO_x anode buffer layers reached 6.57% under illumination which was better than a device performed with PEDOT:PSS HTL. [117] Table 6 summarizes the performances of several BHJ devices using different interfacial layers.

Interestingly, when compared with PEDOT:PSS-based solar cells, devices fabricated using solution processed MoO_x anode buffer layers exhibited much superior stability and longer lifetime after 840 h from being stored in a nitrogen filled glovebox. PCEs of PEDOT:PSS-based devices lost around 88% of their initial value. This degradation was found to occur due to the residual moisture in PEDOT:PSS, which caused corrosion of the cathode layer. On the contrary, devices using MoO_x were found to show dramatically improved stabilities retaining 94% of their initial PCEs [117].

Another team used the same sol-gel process with the same $MoO_2(acac)_2$ precursor but this time the impact of thermal annealing on the work function was studied. It was demonstrated that annealing MoO_x layers has increased the WF from 4.9 eV to 5.3 eV. Consequently, the efficiency of regular P3HT:PC60BM-based cells was improved from 1.3% up to 3.3%. This efficiency was comparable to that of reference PEDOT:PSS-based devices having 3.2%. It is worth noting that the layer morphology of the solution processed MoO_x remained unaffected after this annealing process [118]. In the same study, the stability of devices after storage in air for more than 15 days was measured. This measurement revealed that devices based on solution processed MoO_x (s- MoO_x) HTLs had improved stability when compared to those incorporating PEDOT:PSS HTLs [118].

$Mo(CO)_3(EtCN)_3$ is another precursor that was spin coated and annealed at 120°C for 10 min in air to give continuous thin films of MoO_x . O_2 -plasma treatment enhanced the efficiency of regular P3HT:PC60BM-based devices from 3.43% to 3.53% and this was explained by the increase in WF from 5.15 eV to 5.38 eV after this oxygen exposure [119].

Doctor blading was also used instead of spin coating for MoO_3 deposition. The layers were thermally annealed at 100°C for 10 min and P3HT:PC60BM blend was spin coated on top of them. The fabricated device showed an efficiency of 2.92% which was slightly lower in performance than those based on PEDOT:PSS (3.23%). The optimized thickness of the MoO_3 layers was 47 nm [120].

Table 4. Summary of the PV parameters of PCDTBT-based devices using either PEDOT:PSS or MoO₃HTLs.

Device	J _{sc} (mA·cm ⁻²)	V _{oc} (V)	FF (%)	PCE ^(a) (%)
40 nm PEDOT:PSS	10.11	0.88	66.9	5.95
6 nm MoO _x	10.81	0.89	65.0	6.22
9 nm MoO _x	10.88	0.89	67.2	6.50
12 nm MoO _x	10.87	0.88	66.7	6.40
22 nm MoO _x	10.51	0.88	66.2	6.12

Table 5. Performances of OSCs based on PDTG-TPD:PC70BM and PDTS-TPD:PC70BM inverted systems.

Polymer	J _{sc} (mA·cm ⁻²)	V _{oc} (V)	FF (%)	Average PCE (%)
PDTG-TPD	12.8/14.1	0.86/0.86	66.8/67.3	7.4/8.1
PDTS-TPO	11.4/13.1	0.90/0.90	64.8/66.5	6.6/7.8

Table 6. Device performances of several OSCs using different HTLs.

Device structure	V _{oc} (V)	J _{sc} (mA·cm ⁻²)	FF (%)	PCE (%)
A (ITO/P3HT:PC ₆₀ BM/Ca/Al)	0.40	9.48	56.9	2.16
B (ITO/PEDOT:PSS/P3HT:PC ₆₀ BM/Ca/Al)	0.59	10.19	62.7	3.77
C (ITO/s-MO _x /P3HT:PC ₆₀ BM/Ca/Al)	0.58	11.16	66.8	4.32
D (ITO/P3HT:IC ₆₀ BA/Ca/Al)	0.84	9.66	55.4	4.41
E (ITO/PEDOT:PSS/P3HT:IC ₆₀ BA/Ca/Al)	0.85	9.52	74.9	6.06
F (ITO/s-MO _x /P3HT:IC ₆₀ BA/Ca/Al)	0.85	10.43	72.1	6.29
G (ITO/s-MO _x /P3HT:IC ₇₀ BA/Ca/Al)	0.84	11.09	70.5	6.57

4.3.3.4 Nickel oxide

Nickel oxide (NiO_x) is the only p-type metal oxide used as hole transport materials in OSCs. Its WF strongly depends on the synthetic method, surface chemistry, crystal orientation and thin film deposition conditions. WF is also dependent on post deposition treatments (thermal annealing or O₂-plasma). It is well reported that NiO_x surface may be constituted of residual undecomposed precursors, adsorbed contaminants, and hydroxyl species [90,94].

Thermal evaporation was used to deposit nickel of various thicknesses onto ITO followed by an oxygen plasma treatment to form NiO_x layers. The maximum PCE obtained for P3HT:PC60BM-based devices was 3.54% with a 1-nm-thick NiO_x layer [121]. Other physical approaches were also employed for thin layer deposition of NiO_x including pulsed laser deposition and sputtering. P3HT:PC60BM-based regular devices with such thin NiO_x HTLs gave efficiencies of 5.2% [122] and 2.8% [123] for both approaches, respectively.

Solution-processed NiO_x HTLs were also developed based on sol-gel process. Steirer *et al.* [124] synthesized NiO_x films by spin coating the nickel organic precursor on ITO substrates followed by annealing at 250°C. P3HT:PC60BM-based devices using these films achieved PCEs around 3.6%.

Recently, nickel acetylacetonate Ni(acac)₂ thin films were treated by thermal annealing to be transformed into NiO_x films. PCDTBT:PC70BM-based devices with an as-cast Ni(acac)₂ layer showed lower performance (0.06%) when compared to the thermally annealed films up to 400°C (PCE of 3.5%). This increase in efficiency is likely due to the thermal decomposition of Ni(acac)₂ to form NiO_x. However, an oxygen plasma treatment prior to annealing at 400°C increased the

efficiency to 5.2%. This is due to the generation of a strong dipole at interfaces caused by an increase in nickel oxyhydroxide (NiOOH) species. This suggests that the annealed precursor was a slightly reduced form of NiO_x and O₂ plasma treatment had oxidized the surface layer. Furthermore, the WF was increased from 3.7 eV for the as-deposited layer to 4.7 eV upon annealing then to 5 eV after O₂-plasma treatment which justify the increase in efficiency [125]. In contrast to the common sol-gel route that requires high temperature post-annealing to convert the precursor into NiO_x films, Zhai *et al.* [126] reported an approach to develop solution-processed NiO_x HTLs at lower processing temperatures. This approach was based on simultaneous UV-ozone (UVO) and thermal annealing treatments for NiO_x layers. UPS and X-ray photoelectron spectroscopy (XPS) results demonstrated that at a temperature below 150°C, the dual-treatment approach enhanced the WF of the as-deposited NiO_x films from 3.7 eV to 5.1 eV. It was believed that UVO treatment alone generated NiOOH species, while the dual treatment further increased the concentration of NiOOH species on the film surface. Due to the suitable WF of the NiO_x films, PBDDT-TPD:PC60BM-based systems showed PCE of 5.09% which was quite higher than those based on PEDOT:PSS HTLs (4.19%). Interestingly, it was proven that the air stability of devices under 1 sun was enhanced by replacing PEDOT:PSS with these NiO_x HTLs.

Combustion reactions were also used as low-temperature approaches to deposit NiO_x thin films starting from an aqueous nickel nitrate solution (oxidizer) and glycine (fuel). A processing temperature, as low as 175°C, was sufficient to initiate the combustion reaction and convert the precursor into oxide thin films. For TQ1:PC70BM OPVs with NiO_x HTLs, an efficiency of 6.42% with a high FF of 70% was obtained in comparison to 5.23% with PEDOT:PSS HTLs [127].

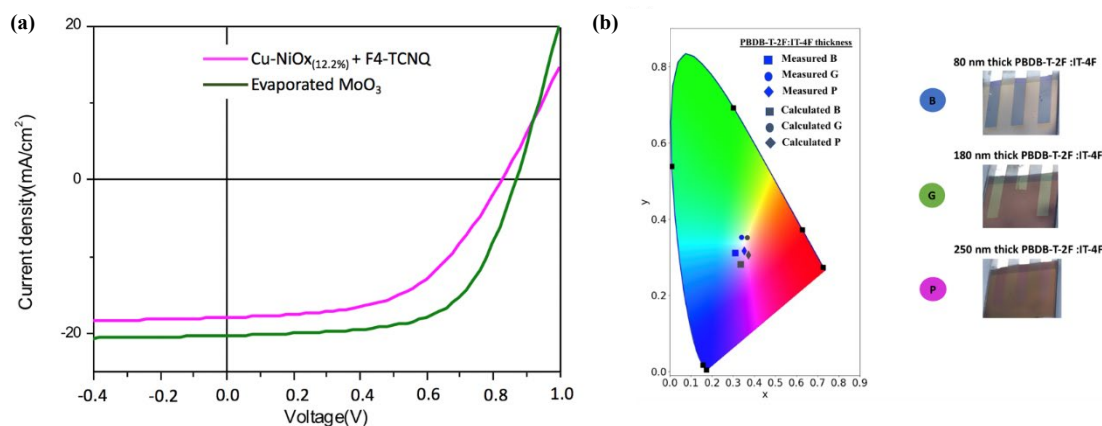


Figure 16. (a) The J - V curves of PBDB-T-2F:IT-4F-based inverted device structures using different HTLs and (b) the color coordinates for the experimental cells (left) along with their photographic images (right). Reproduced from Ref. 134 with permission from the Royal Society of Chemistry.

To avoid precursor approaches, [Zhiyuan Xie *et al.*](#) [128] proposed the first annealing-free sonochemical synthesis to prepare NiO_x nanoparticles. The colloidal NiO_x nanocrystals were prepared starting from nickel chloride (NiCl₂) at low temperature via ultrasonic irradiation. These nanoparticles were directly spin coated without any post-thermal annealing, making it compatible with flexible substrates and low-cost fabrications. The PCE of PCDTBT:PC70BM-based devices was increased from 5.84% to 6.30% by replacing PEDOT:PSS with the O₂-plasma treated NiO_x HTLs. The device stability was also enhanced.

During some synthesis, ligands were often needed to disperse and stabilize the metal oxide nanocrystals (NCs). For instance, [Liang *et al.*](#) [129] reported lithium stearate stabilized NiO_x nanocrystals as HTLs for OSCs. TQ1:PC70BM-based devices achieved an average PCE of 6.1% using the UVO treated NiO_x layers. This treatment is essential to remove the insulating surface ligands and to increase the WF of the NiO_x films.

Choy's group demonstrated post-treatment-free NiO_x NCs by a facile chemical precipitation method. These results were completely different from the previously reported ones as they claimed the presence of NiOOH species on the surface without any UVO or O₂-plasma treatment. The as-deposited NiO_x films possess a WF of 5.25 eV which favored an Ohmic contact with the HOMO level of the donor. NiO_x nanoparticles dispersed in water were used as HTLs for fabricating PTB7-Th:PC70BM-based OSCs with 9.16% efficiency. This PCE overwhelmed the conventional PEDOT:PSS-based devices having a PCE of 8.6%. The series resistance for the NiO_x-based devices was less than that with PEDOT:PSS resulting in better electrical contacts and FF [130].

Interestingly, solution processed NiO_x nanoparticles can be used for large scale fabrication as reported by [Garg *et al.*](#) [131]. Very thin NiO_x films were ink-jet printed, thermally treated at 400°C then UVO treated. When integrated into P3HT:PC60BM-based devices, PCE of 2.59% was obtained. This was comparable to those devices based on spin coated NiO_x films (2.28%).

The low conductivity of NiO_x HTLs will dramatically affect performance of OSCs by increasing recombination and reducing hole extraction. Additionally, the low series resistance will limit deposition to only thin layers which are not suitable for large-scale

fabrication. Thus, metal ion doping is an effective approach to increase conductivity for better hole extraction, transport and collection [132, 133]. [Alkarsifi *et al.*](#) [134] developed a strategy to produce chemically precipitated copper doped NiO_x NPs that form aggregate-free isopropanol solution suitable for processing on top of photoactive layers. Further doping of these nanoparticles with an organic electron acceptor, namely 2,3,5,6-tetrafluoro-7,7,8,8-tetra-cyanoquinodimethane (F4-TCNQ) was necessary to tune the WF from 4.47 eV to 5.45 eV, favoring an energy level alignment of Cu-NiO_x with several donor materials. The doped NiO_x NPs form highly effective HTLs for regular device structures, leading to PCEs of 7.4% in PTB7:PC70BM blends. When applied to NFA-based solar cells using PBDB-T-2F:IT-4F with an inverted device structure, these hybrid HTLs lead to a PCE of 7.9% compared to 11% obtained with evaporated MoO_x and 6.3% reached with PEDOT:PSS (Figure 16(a)). These Cu-NiO_x HTLs can be processed up to 45 nm without inducing electric losses due to optimized WF and high conductivity.

Interestingly, they demonstrated that Cu-NiO_x HTLs can introduce the so-called optical spacer effects in inverted device structures that were so far only reported in regular structures using ETLs (such as ZnO) [35]. These OSPs can modify light distribution inside devices and allow for color tuning over a large palette (Figure 16(b)).

5. Conclusion

Achieving both high efficiency and stability remains a challenge for organic solar cells. On this way, tremendous progress has been done on various levels, with noticeable improvements of the active layer materials, the device structure, the fabrication processes and the interfacial engineering. Concerning the interfaces, the Hole Transport Layer is still subject to a large amount of research in order to adequately address all the expected requirements for such a layer, mainly the efficient charge (holes) selectivity and transport for ensuring the performances together with a suitable behavior regarding the degradation issues. A large number of materials has been reported so far, some of them been clearly identified as good candidates such as graphene oxide, organic conducting polymers or transition metal oxides. Amongst them, PEDOT:PSS as HTL could lead to OSCs with the actual record PCE above 19% while modified e-MoO₃

allowed for OSCs having operating lifetime surpassing decades. The elaboration of new composite materials may be the key for obtaining HTL combining the different advantages of each, even though the fabrication easiness could be affected. There would be still many challenges remaining in the field of HTL elaboration, such as ensuring a possibility for large-scale manufacturing, while addressing some additional properties that are very specific to OPV: the color management and device stretchability.

Acknowledgements

The authors thank the french Ministere de l'Enseignement Supérieur, de la Recherche et de l'Innovation for Ph.D. grant funding for RA.

References

- [1] H. Kim, S. Nam, J. Jeong, S. Lee, J. Seo, H. Han, and Y. Kim, "Organic solar cells based on conjugated polymers : History and recent advances" *Korean Journal of Chemical Engineering*, vol. 31, no. 7, pp. 1095-1104, 2014.
- [2] M. Grätzel, "Photoelectrochemical cells" *Nature*, vol. 414, no. 6861, p. 338, 2001.
- [3] M. C. Scharber, and N. S. Sariciftci, "Efficiency of bulk-heterojunction organic solar cells," *Progress in Polymer Science*, vol. 38, no. 12, pp. 1929-1940, 2013.
- [4] M. Hösel, D. Angmo, and F. C. Krebs, "17 - Organic solar cells (OSCs)" in *Handbook of Organic Materials for Optical and (Opto)electronic Devices*, O. Ostroverkhova, Ed. Woodhead Publishing, 2013, pp. 473-507.
- [5] K. Y. Mitra, A. Alalawe, S. Voigt, C. Boeffel, and R. R. Baumann, "Manufacturing of all inkjet-printed organic photovoltaic cell arrays and evaluating their suitability for flexible electronics" *Micromachines (Basel)*, vol. 9, no. 12, 2018.
- [6] K. Chong, X. Xu, H. Meng, J. Xue, L. Yu, W. Ma, and Q. Peng, "Realizing 19.05% efficiency polymer solar cells by progressively improving charge extraction and suppressing charge recombination" *Advanced Materials*, vol. 34, no. 13, p. 2109516, 2022.
- [7] D. Landerer, A. Mertens, D. Freis, R. Droll, T. Leonhard, A. D. Schulz, D. Bahro, and A. Colmann, "Enhanced thermal stability of organic solar cells comprising ternary D-D-A bulk-heterojunctions" *npj Flexible Electronics*, vol. 1, no. 1, 2017.
- [8] Y. Li, X. Huang, K. Ding, H. K. M. Sheriff Jr, L. Ye, H. Liu, C.-Z. Li, H. Ade, and S. R. Forrest, "Non-fullerene acceptor organic photovoltaics with intrinsic operational lifetimes over 30 years" *Nature Communications*, vol. 12, no. 1, Art. no. 1, 2021.
- [9] A. Henemann, "BIPV: Built-in solar energy" *Renewable Energy Focus*, vol. 9, no. 6, pp. 14-19, 2008.
- [10] S. Almosni, A. Delamarre, Z. Jehl, D. Suchet, L. Cojocar, M. Giteau, B. Behaghel, A. Julian, C. Ibrahim, L. Tetry, H. Wang, T. Kubo, S. Uchida, H. Segawa, N. Miyashita, R. Tamaki, Y. Shoji, K. Yoshida, N. Ahsan, K. Watanabe, T. Inoue, M. Sugiyama, Y. Nakano, T. Hamamura, T. Toupance, C. Olivier, S. Chambon, L. Vignau, C. Geffroy, E. Cloutet, G. Hadziioannou, N. Cavassilas, P. Rale, A. Cattoni, S. Collin, F. Gibelli, M. Paire, L. Lombez, D. Aureau, M. Bouttemy, A. Etcheberry, Y. Okada, and J.-F. Guillemoles, "Material challenges for solar cells in the twenty-first century: directions in emerging technologies" *Science and Technology of Advanced Materials*, vol. 19, no. 1, pp. 336-369, 2018.
- [11] R. Das, "Organic Photovoltaics (OPV) 2013-2023: Technologies, Markets, Players: IDTechEx" Apr. 10, 2013.
- [12] F. J. Zhang, D. W. Zhao, Z. L. Zhuo, H. Wang, Z. Xu, and Y. S. Wang, "Inverted small molecule organic solar cells with Ca modified ITO as cathode and MoO₃ modified Ag as anode" *Solar Energy Materials and Solar Cells*, vol. 94, no. 12, pp. 2416-2421, 2010.
- [13] R. Po, C. Carbonera, A. Bernardi, and N. Camaioni, "The role of buffer layers in polymer solar cells" *Energy & Environmental Science*, vol. 4, no. 2, pp. 285-310, 2011.
- [14] S. Savagatrup, A. D. Printz, T. F. O'Connor, A. V Zaretski, D. Rodriguez, E. J. Sawyer, K. M. Rajan, R. I. Acosta, S. E. Root, and D. J. Lipomi, "Mechanical degradation and stability of organic solar cells: molecular and microstructural determinants" *Energy & Environmental Science*, vol. 8, no. 1, pp. 55-80, 2014.
- [15] E. Pavlopoulou, G. Fleury, D. Deribew, F. Cousin, M. Geoghegan, and G. Hadziioannou, "Phase separation-driven stratification in conventional and inverted P3HT:PCBM organic solar cells" *Organic Electronics*, vol. 14, no. 5, pp. 1249-1254, 2013.
- [16] H. You, L. Dai, Q. Zhang, D. Chen, Q. Jiang, and C. Zhang, "Enhanced performance of inverted non-fullerene organic solar cells by using metal oxide electron- and hole-selective layers with process temperature ≤ 150 °C" *Polymers*, vol. 10, no. 7, Art. no. 7, 018.
- [17] Y. Udum, P. Denk, G. Adam, D. H. Apaydin, A. Nevsad, C. Teichert, M. S White, and N. S Sariciftci, "Inverted bulk-heterojunction solar cell with cross-linked hole-blocking layer" *Organic Electronics*, vol. 15, no. 5, pp. 997-1001, 2014.
- [18] N. Sharma, C. M. S. Negi, V. Yadav, A. S. Verma, V. Sadhu, and S. K. Gupta, "Inverted organic solar cells based on PTB7: PC70BM bulk heterojunction" *AIP Conference Proceedings*, vol. 2100, no. 1, p. 020061, 2019.
- [19] Y. Cui, H. Yao, J. Zhang, T. Zhang, Y. Wang, L. Hong, K. Xian, B. Xu, S. Zhang, J. Peng, Z. Wei, F. Gao, and J. Hou, "Over 16% efficiency organic photovoltaic cells enabled by a chlorinated acceptor with increased open-circuit voltages" *Nature Communications*, vol. 10, 2019.
- [20] G. Sauvé, and R. Fernando, "Beyond fullerenes: Designing alternative molecular electron acceptors for solution-processable bulk heterojunction organic photovoltaics" *The Journal of Physical Chemistry Letters*, vol. 6, no. 18, pp. 3770-3780, 2015.
- [21] W. Cao, and J. Xue, "Recent progress in organic photovoltaics: device architecture and optical design" *Energy & Environmental Science*, vol. 7, no. 7, p. 2123, 2014.
- [22] S. Kouijzer, J. J. Michels, M. van den Berg, V. S. Gevaerts, M. Turbiez, M. M. Wienk, and R. A. J. Janssen, "Predicting morphologies of solution processed polymer:fullerene blends" *Journal of the American Chemical Society*, vol. 135, no. 32, pp. 12057-12067, 2013.

- [23] S. Bi, Z. Ouyang, S. Shaik, and D. Li, "Effect of donor-acceptor vertical composition profile on performance of organic bulk heterojunction solar cells" *Scientific Reports*, vol. 8, no. 1, p. 9574, 2018.
- [24] W. Ma, C. Yang, X. Gong, K. Lee, and A. J. Heeger, "Thermally stable, efficient polymer solar cells with nanoscale control of the interpenetrating network morphology" *Advanced Functional Materials*, vol. 15, no. 10, pp. 1617-1622, 2005.
- [25] G. Li, V. Shrotriya, J. Huang, Y. Yao, T. Moriarty, K. Emery, and Y. Yang, "High-efficiency solution processable polymer photovoltaic cells by self-organization of polymer blends" *Nature Materials*, vol. 4, no. 11, p. 864, 2005.
- [26] Y. Yao, J. Hou, Z. Xu, G. Li, and Y. Yang, "Effects of solvent mixtures on the nanoscale phase separation in polymer solar cells: effect of solvent mixture on nanoscale phase separation in polymer solar cells" *Advanced Functional Materials*, vol. 18, no. 12, pp. 1783-1789, 2008.
- [27] J. Peet, J. Y. Kim, N. E. Coates, W. L. Ma, D. Moses, A. J. Heeger, and G. C. Bazan, "Efficiency enhancement in low-bandgap polymer solar cells by processing with alkane dithiols" *Nature Materials*, vol. 6, no. 7, pp. 497-500, 2007.
- [28] H.-C. Liao, C.-C. Ho, C.-Y. Chang, M.-H. Jao, S. B. Darling, and W.-F. Su, "Additives for morphology control in high-efficiency organic solar cells" *Materials Today*, vol. 16, no. 9, pp. 326-336, 2013.
- [29] S. B. Dkhil, M. Pfannmöller, M. I. Saba, M. Gaceur, H. Heidari, C. Vidélot-Ackermann, O. Margeat, A. Guerrero, J. Bisquert, G. Garcia-Belmonte, A. Mattoni, S. Bals, and J. Ackermann, "Toward high-temperature stability of PTB7-based bulk heterojunction solar cells: impact of fullerene size and solvent additive" *Advanced Energy Materials*, vol. 7, no. 4, p. 1601486, 2017.
- [30] S. J. Lou, J. M. Szarko, T. Xu, L. Yu, T. J. Marks, and L. X. Chen, "Effects of additives on the morphology of solution phase aggregates formed by active layer components of high-efficiency organic solar cells" *Journal of the American Chemical Society*, vol. 133, no. 51, pp. 20661-20663, 2011.
- [31] B. A. Collins, Z. Li, J. R. Tumbleston, E. Gann, C. R. McNeill, and H. Ade, "Absolute measurement of domain composition and nanoscale size distribution explains performance in PTB7:PC71BM solar cells" *Advanced Energy Materials*, vol. 3, no. 1, pp. 65-74, 2013.
- [32] T. Zhuang, X.-F. Wang, T. Sano, Z. Hong, Y. Yang, and J. Kido, "Fullerene derivatives as electron donor for organic photovoltaic cells" *Applied Physics Letters*, vol. 103, no. 20, p. 203301, 2013.
- [33] R. C. Chiechi, R. W. A. Havenith, and J. C. Hummelen, "Modern plastic solar cells: materials, mechanisms and modeling" *Materials Today*, vol. 16, no. 7-8, pp. 281-289, 2013.
- [34] A. K. Vivek, and G. D. Agrawal, "Organic solar cells: principles, mechanism and recent developments" *International Journal of Research in Engineering and Technology*, vol. 03, no. 09, pp. 338-341, 2014.
- [35] H. Sun, F. Chen, and Z.-K. Chen, "Recent progress on non-fullerene acceptors for organic photovoltaics" *Materials Today*, vol. 24, pp. 94-118, 2019.
- [36] C. Soci, I.-W. Hwang, D. Moses, Z. Zhu, D. Waller, R. Gaudiana, C. J. Brabec, and A. J. Heeger, "Photoconductivity of a low-bandgap conjugated polymer" *Advanced Functional Materials*, vol. 17, no. 4, pp. 632-636, 2007.
- [37] G. D. Sharma, M. Anil Reddy, D. V Ramana, and M. Chandrasekharam, "A novel carbazole-phenothiazine dyad small molecule as a non-fullerene electron acceptor for polymer bulk heterojunction solar cells" *RSC Advances*, vol. 4, no. 63, pp. 33279-33285, 2014.
- [38] Q. Peng, T. Liang, and Kui Feng, "Design of low bandgap conjugated polymers for organic solar cell application" 2013.
- [39] J. Peet, J. Y. Kim, N. E. Coates, W. L. Ma, D. Moses, A. J. Heeger, and G. C. Bazan, "Efficiency enhancement in low-bandgap polymer solar cells by processing with alkane dithiols" *Nature Materials*, vol. 6, no. 7, pp. 497-500, 2007.
- [40] J. S. Moon, J. Jo, and A. J. Heeger, "Nanomorphology of PCDTBT:PC70BM Bulk Heterojunction Solar Cells" *Advanced Energy Materials*, vol. 2, no. 3, pp. 304-308, 2012.
- [41] S. H. Park, A. Roy, S. Beaupré, S. Cho, N. Coates, J. S. Moon, D. Moses, M. Leclerc, K. Lee, and A. J. Heeger, "Bulk heterojunction solar cells with internal quantum efficiency approaching 100%" *Nature Photonics*, vol. 3, no. 5, pp. 297-302, May 2009.
- [42] L. Song, W. Wang, E. Barabino, D. Yang, V. Körstgens, P. Zhang, S. V Roth, and P. Müller-Buschbaum, "Composition-morphology correlation in PTB7-Th/PC71BM blend films for organic solar cells" *ACS Applied Materials & Interfaces*, vol. 11, no. 3, pp. 3125-3135, 2019.
- [43] L. Lu, and L. Yu, "Understanding low bandgap polymer PTB7 and optimizing polymer solar cells based on it" *Advanced Materials*, vol. 26, no. 26, pp. 4413-4430, 2014.
- [44] S. Ben Dkhil, M. Pfannmöller, S. Bals, T. Koganezawa, N. Yoshimoto, D. Hannani, M. Gaceur, C. Vidélot-Ackermann, O. Margeat, and J. Ackermann, "Square-centimeter-sized high-efficiency polymer solar cells: How the processing atmosphere and film quality influence performance at large scale" *Advanced Energy Materials*, vol. 6, no. 13, p. 1600290, 2016.
- [45] Y. Liu, J. Zhao, Z. Li, C. Mu, W. Ma, H. Hu, K. Jiang, H. Lin, H. Ade, and H. Yan, "Aggregation and morphology control enables multiple cases of high-efficiency polymer solar cells" *Nature Communications*, vol. 5, no. 1, 2014.
- [46] J. Zhao, Y. Li, G. Yang, K. Jiang, H. Lin, H. Ade, W. Ma, and H. Yan, "Efficient organic solar cells processed from hydrocarbon solvents" *Nature Energy*, vol. 1, no. 2, p. 15027, 2016.
- [47] H. Spanggaard, and F. C. Krebs, "A brief history of the development of organic and polymeric photovoltaics" *Solar Energy Materials And Solar Cells*, vol. 83, no. 2-3, pp. 125-146, 2004.
- [48] E. von Hauff, V. Dyakonov, and J. Parisi, "Study of field effect mobility in PCBM films and P3HT : PCBM blends" *Solar Energy Materials And Solar Cells*, vol. 87, no. 1-4, pp. 149-156, May 2005.
- [49] H. Xin, X. Guo, G. Ren, M. D. Watson, and S. A. Jenekhe, "Efficient phthalimide copolymer-based bulk heterojunction solar cells: How the Processing additive influences nanoscale

- morphology and photovoltaic properties” *Advanced Energy Materials*, vol. 2, no. 5, pp. 575–582, 2012.
- [50] P. Cheng, G. Li, X. Zhan, and Y. Yang, “Next-generation organic photovoltaics based on non-fullerene acceptors” *Nature Photonics*, vol. 12, no. 3, pp. 131–142, 2018.
- [51] Y. He, and Y. Li, “Fullerene derivative acceptors for high performance polymer solar cells” *Physical Chemistry Chemical Physics*, vol. 13, no. 6, pp. 1970–1983, 2011.
- [52] M. Jørgensen, K. Norrman, S. A. Gevorgyan, T. Tromholt, B. Andreasen, and F. C. Krebs, “Stability of polymer solar cells” *Advanced Materials*, vol. 24, no. 5, pp. 580–612, 2012.
- [53] P. Cheng, and X. Zhan, “Stability of organic solar cells: challenges and strategies” *Chemical Society Reviews*, vol. 45, no. 9, pp. 2544–2582, 2016.
- [54] A. Polman, M. Knight, E. C. Garnett, B. Ehrler, and W. C. Sinke, “Photovoltaic materials: Present efficiencies and future challenges” *Science*, vol. 352, no. 6283, p. aad4424, 2016.
- [55] M. T. Dang, L. Hirsch, and G. Wantz, “P3HT:PCBM, best seller in polymer photovoltaic research” *Advanced Materials*, vol. 23, no. 31, pp. 3597–3602, A2011.
- [56] C. Yan, S. Barlow, Z. Wang, H. Yan, A. K.-Y. Jen, S. R. Marder, and X. Zhan, “Non-fullerene acceptors for organic solar cells” *Nature Reviews Materials*, vol. 3, p. 18003, 2018.
- [57] W. Zhao, S. Li, H. Yao, S. Zhang, Y. Zhang, B. Yang, and J. Hou, “Molecular optimization enables over 13% efficiency in organic solar cells” *Journal of the American Chemical Society*, vol. 139, no. 21, pp. 7148–7151, 2017.
- [58] H. Zhang, H. Yao, J. Hou, J. Zhu, J. Zhang, W. Li, R. Yu, B. Gao, S. Zhang, and J. Hou, “Over 14% efficiency in organic solar cells enabled by chlorinated nonfullerene small-molecule acceptors” *Advanced Materials*, vol. 30, no. 28, p. e1800613, 2018.
- [59] C.-C. Chueh, C.-Z. Li, and A. K.-Y. Jen, “Recent progress and perspective in solution-processed Interfacial materials for efficient and stable polymer and organometal perovskite solar cells” *Energy & Environmental Science*, vol. 8, no. 4, pp. 1160–1189, 2015.
- [60] S. Ben Dkhil, M. Pfannmöller, S. Bals, T. Koganezawa, N. Yoshimoto, D. Hannani, M. Gaceur, C. Videlot-Ackermann, O. Margeat, and J. Ackermann, “Square-centimeter-sized high-efficiency polymer solar cells: How the processing atmosphere and film quality influence performance at large scale” *Advanced Energy Materials*, vol. 6, no. 13, p. 1600290, 2016.
- [61] M. Li, W. Ni, B. Kan, X. Wan, L. Zhang, Q. Zhang, G. Long, Y. Zuo, and Y. Chen, “Graphene quantum dots as the hole transport layer material for high-performance organic solar cells” *Physical Chemistry Chemical Physics*, vol. 15, no. 43, pp. 18973–18978, 2013.
- [62] C.-C. Chueh, C.-Z. Li, and A. K.-Y. Jen, “Recent progress and perspective in solution-processed Interfacial materials for efficient and stable polymer and organometal perovskite solar cells” *Energy & Environmental Science*, vol. 8, no. 4, pp. 1160–1189, Apr. 2015.
- [63] G. Garcia-Belmonte, A. Munar, E. M. Barea, J. Bisquert, I. Ugarte, and R. Pacios, “Charge carrier mobility and lifetime of organic bulk heterojunctions analyzed by impedance spectroscopy” *Organic Electronics*, vol. 9, no. 5, pp. 847–851, 2008.
- [64] V. D. Mihailetschi, P. W. M. Blom, J. C. Hummelen, and M. T. Rispen, “Cathode dependence of the open-circuit voltage of polymer:fullerene bulk heterojunction solar cells” *Journal of Applied Physics*, vol. 94, no. 10, pp. 6849–6854, 2003.
- [65] A. Mityashin, D. Cheyins, B. P. Rand, and P. Heremans, “Understanding metal doping for organic electron transport layers” *Applied Physics Letters*, vol. 100, no. 5, p. 053305, 2012.
- [66] M. Gaceur, S. Ben Dkhil, D. Duché, F. Bencheikh, J.-J. Simon, L. Escoubas, M. Mansour, A. Guerrero, G. Garcia-Belmonte, X. Liu, M. Fahlman, W. Dachraoui, A. K. Diallo, C. Videlot-Ackermann, O. Margeat, and J. Ackermann, “Ligand-free synthesis of aluminum-doped zinc oxide nanocrystals and their use as optical spacers in color-tuned highly efficient organic solar cells” *Advanced Functional Materials*, vol. 26, no. 2, pp. 243–253, 2016.
- [67] S. Lattante, “Electron and hole transport layers: their use in inverted bulk heterojunction polymer solar cells” *Electronics*, vol. 3, no. 1, pp. 132–164, -2014.
- [68] H.-L. Yip, and A. K.-Y. Jen, “Recent advances in solution-processed interfacial materials for efficient and stable polymer solar cells” *Energy & Environmental Science*, vol. 5, no. 3, pp. 5994–6011, 2012.
- [69] P. W. M. Blom, V. D. Mihailetschi, L. J. A. Koster, and D. E. Markov, “Device physics of polymer:fullerene bulk heterojunction solar cells” *Advanced Materials*, vol. 19, no. 12, pp. 1551–1566, 2007.
- [70] C.-Z. Li, H.-L. Yip, and A. K.-Y. Jen, “Functional fullerenes for organic photovoltaics” *Journal of Materials Chemistry*, vol. 22, no. 10, pp. 4161–4177, 2012.
- [71] C.-Z. Li, C.-C. Chueh, H.-L. Yip, K. M. O’Malley, W.-C. Chen, and A. K.-Y. Jen, “Effective interfacial layer to enhance efficiency of polymer solar cells via solution-processed fullerene-surfactants” *Journal of Materials Chemistry*, vol. 22, no. 17, pp. 8574–8578, 2012.
- [72] R. Steim, F. R. Kogler, and C. J. Brabec, “Interface materials for organic solar cells” *Journal of Materials Chemistry*, vol. 20, no. 13, pp. 2499–2512, 2010.
- [73] N. Camaioni, and R. Po, “Pushing the envelope of the intrinsic limitation of organic solar cells” *The Journal of Physical Chemistry Letters*, vol. 4, no. 11, pp. 1821–1828, 2013.
- [74] S. Ben Dkhil, D. Duché, M. Gaceur, A. K. Thakur, F. B. Aboura, L. Escoubas, J.-J. Simon, A. Guerrero, J. Bisquert, G. Garcia-Belmonte, Q. Bao, M. Fahlman, C. Videlot-Ackermann, O. Margeat, and J. Ackermann, “Interplay of optical, morphological, and electronic effects of ZnO optical spacers in highly efficient polymer solar cells” *Advanced Energy Materials*, vol. 4, no. 18, p. 1400805, 2014.
- [75] K. Suemori, M. Yokoyama, and M. Hiramoto, “Electrical shorting of organic photovoltaic films resulting from metal migration” *Journal of Applied Physics*, vol. 99, no. 3, p. 036109, F2006.
- [76] G. Wantz, L. Hirsch, N. Huby, L. Vignau, J. F. Silvain, A. S. Barrière, and J. P. Parneix, “Correlation between the Indium

- Tin Oxide morphology and the performances of polymer light-emitting diodes" *Thin Solid Films*, vol. 485, no. 1-2, pp. 247-251, 2005.
- [77] K. Lee, J. Y. Kim, S. H. Park, S. H. Kim, S. Cho, and A. J. Heeger, "Air-Stable polymer electronic devices" *Advanced Materials*, vol. 19, no. 18, pp. 2445-2449, 2007.
- [78] K.-H. Tu, S.-S. Li, W.-C. Li, D.-Y. Wang, J.-R. Yang, and C.-W. Chen, "Solution processable nanocarbon platform for polymer solar cells" *Energy & Environmental Science*, vol. 4, no. 9, p. 3521, 2011.
- [79] C. T. G. Smith, R. W. Rhodes, M. J. Beliatis, K. D. G. Imalka Jayawardena, L. J. Rozanski, C. A. Mills, and S. R. P. Silva, "Graphene oxide hole transport layers for large area, high efficiency organic solar cells" *Applied Physics Letters*, vol. 105, no. 7, p. 073304, 2014.
- [80] L. Zhou, D. Yang, W. Yu, J. Zhang, and C. Li, "An efficient polymer solar cell using graphene oxide interface assembled via layer-by-layer deposition" *Organic Electronics*, vol. 23, pp. 110-115, 2015.
- [81] S. Mao, H. Pu, and J. Chen, "Graphene oxide and its reduction: modeling and experimental progress" *RSC Advances*, vol. 2, no. 7, pp. 2643-2662, 2012.
- [82] S. Rafique, N. A. Roslan, S. M. Abdullah, L. Li, A. Supangat, A. Jilani, and M. Iwamoto, "UV- ozone treated graphene oxide/ PEDOT:PSS bilayer as a novel hole transport layer in highly efficient and stable organic solar cells" *Organic Electronics*, vol. 66, pp. 32-42, 2019.
- [83] X. Ouyang, R. Peng, L. Ai, X. Zhang, and Z. Ge, "Efficient polymer solar cells employing a non-conjugated small-molecule electrolyte" *Nature Photonics*, vol. 9, no. 8, pp. 520-524, 2015.
- [84] V. Gupta, A. K. K. Kyaw, D. H. Wang, S. Chand, G. C. Bazan, and A. J. Heeger, "Barium: An efficient cathode layer for bulk-heterojunction solar cells" *Scientific Reports*, vol. 3, no. 1, p. 1965, 2013.
- [85] Z. Tan, S. Li, F. Wang, D. Qian, J. Lin, J. Hou, and Y. Li, "High performance polymer solar cells with as-prepared zirconium acetylacetonate film as cathode buffer layer" *Scientific Reports*, vol. 4, no. 1, p. 4691, 2015.
- [86] Z. Tan, L. Li, C. Li, L. Yan, F. Wang, J. Xu, L. Yu, B. Song, J. Hou, and Y. Li, "Trapping light with a nanostructured CeO_x/Al back electrode for high-performance polymer solar cells" *Advanced Materials Interfaces*, vol. 1, no. 8, p. 1400197, 2014.
- [87] S. Shao, J. Liu, J. Bergqvist, S. Shi, C. Veit, U. Würfel, Z. Xie, and F. Zhang, "In Situ Formation of MoO₃ in PEDOT: PSS Matrix: A facile way to produce a smooth and less hygroscopic hole transport layer for highly stable polymer bulk heterojunction solar cells" *Advanced Energy Materials*, vol. 3, no. 3, pp. 349-355, 2013.
- [88] H. Bin, T. P. A. van der Pol, J. Li, B. T. van Gorkom, M. M. Wienk, and R. A. J. Janssen, "Efficient organic solar cells with small energy losses based on a wide-bandgap trialkylsilyl-substituted donor polymer and a non-fullerene acceptor" *Chemical Engineering Journal*, vol. 435, p. 134878, 2022.
- [89] Y. Cui, Y. Xu, H. Yao, P. Bi, L. Hong, J. Zhang, Y. Zu, T. Zhang, J. Qin, J. Ren, Z. Chen, C. He, X. Hao, Z. Wei, and J. Hou, "Single-Junction Organic Photovoltaic Cell with 19% Efficiency" *Advanced Materials*, vol. 33, no. 41, p. 2102420, 2021.
- [90] F. Wang, Z. Tan, and Y. Li, "Solution-processable metal oxides/chelates as electrode buffer layers for efficient and stable polymer solar cells" *Energy & Environmental Science*, vol. 8, no. 4, pp. 1059-1091, 2015.
- [91] W.-H. Baek, M. Choi, T.-S. Yoon, H. H. Lee, and Y.-S. Kim, "Use of fluorine-doped tin oxide instead of indium tin oxide in highly efficient air-fabricated inverted polymer solar cells" *Applied Physics Letters*, vol. 96, no. 13, p. 133506, 2010.
- [92] Y.-J. Cheng, C.-H. Hsieh, Y. He, C.-S. Hsu, and Y. Li, "Combination of Indene-C60 Bis-adduct and cross-linked fullerene interlayer leading to highly efficient inverted polymer solar cells" *Journal of the American Chemical Society*, vol. 132, no. 49, pp. 17381-17383, 2010.
- [93] S. K. Hau, H.-L. Yip, H. Ma, and A. K.-Y. Jen, "High performance ambient processed inverted polymer solar cells through interfacial modification with a fullerene self-assembled monolayer" *Applied Physics Letters*, vol. 93, no. 23, p. 233304, 2008.
- [94] S. Chen, J. R. Manders, S.-W. Tsang, and F. So, "Metal oxides for interface engineering in polymer solar cells" *Journal of Materials Chemistry*, vol. 22, no. 46, p. 24202, 2012.
- [95] J. Meyer, S. Hamwi, M. Kröger, W. Kowalsky, T. Riedl, and A. Kahn, "Transition metal oxides for organic electronics: energetics, device physics and applications" *Advanced Materials*, vol. 24, no. 40, pp. 5408-5427, Oct. 2012.
- [96] X. Liang, S. Bai, X. Wang, X. Dai, F. Gao, B. Sun, Z. Ning, Z. Ye, and Y. Jin, "Colloidal metal oxide nanocrystals as charge transporting layers for solution-processed light-emitting diodes and solar cells" *Chemical Society Reviews*, vol. 46, no. 6, pp. 1730-1759, 2017.
- [97] S. Lattante, "Electron and Hole transport layers: Their use in inverted bulk heterojunction polymer solar cells" *Electronics*, vol. 3, no. 1, pp. 132-164, 2014.
- [98] K. Zilberberg, S. Trost, H. Schmidt, and T. Riedl, "Solution processed vanadium pentoxide as charge extraction layer for organic solar cells" *Advanced Energy Materials*, vol. 1, no. 3, pp. 377-381, 2011.
- [99] C.-P. Chen, Y.-D. Chen, and S.-C. Chuang, "High-performance and highly durable inverted organic photovoltaics embedding solution-processable vanadium oxides as an interfacial hole-transporting layer" *Advanced Materials*, vol. 23, no. 33, pp. 3859-3863, 2011.
- [100] X. Bao, Q. Zhu, T. Wang, J. Guo, C. Yang, D. Yu, N. Wang, W. Chen, and R. Yang, "Simple O₂ plasma-processed V₂O₅ as an anode buffer layer for high-performance polymer solar cells" *ACS Applied Materials & Interfaces*, vol. 7, no. 14, pp. 7613-7618, 2015.
- [101] K. Zilberberg, S. Trost, J. Meyer, A. Kahn, A. Behrendt, D. Lützenkirchen-Hecht, R. Frahm, and T. Riedl, "Inverted organic solar cells with sol-gel processed high work-function vanadium oxide hole-extraction layers," *Advanced Functional Materials*, vol. 21, no. 24, pp. 4776-4783, 2011.
- [102] Z. Tan, W. Zhang, C. Cui, Y. Ding, D. Qian, Q. Xu, L. Li, S. Li, and Y. Li, "Solution-processed vanadium oxide as a hole

- collection layer on an ITO electrode for high-performance polymer solar cells" *Physical Chemistry Chemical Physics*, vol. 14, no. 42, pp. 14589-14595, 2012.
- [103] F. Xie, W. C. H. Choy, C. Wang, X. Li, S. Zhang, J. Hou, "Low-Temperature solution-processed hydrogen molybdenum and vanadium bronzes for an efficient hole-transport layer in organic electronics" *Advanced Materials*, vol. 25, no. 14, pp. 2051-2055, 2013.
- [104] X. Li, F. Xie, S. Zhang, J. Hou, and W. C. H. Choy, "Over 1.1 eV work function tuning of cesium intercalated metal oxides for functioning as both electron and hole transport layers in organic optoelectronic devices" *Advanced Functional Materials*, vol. 24, no. 46, pp. 7348-7356, 2014.
- [105] S.-P. Cho, J.-S. Yeo, D.-Y. Kim, S. Na, and S.-S. Kim, "Brush painted V₂O₅ hole transport layer for efficient and air-stable polymer solar cells" *Solar Energy Materials and Solar Cells*, vol. 132, pp. 196-203, 2015.
- [106] X. Yang, E. Mutlugun, Y. Zhao, Y. Gao, K. S. Leck, Y. Ma, L. Ke, S. T. Tan, H. V. Demir, and X. W. Sun, "Solution processed tungsten oxide interfacial layer for efficient hole-injection in quantum dot light-emitting diodes" *Small*, vol. 10, no. 2, pp. 247-252, 2014.
- [107] C. Tao, S. Ruan, G. Xie, X. Kong, L. Shen, F. Meng, C. Liu, X. Zhang, W. Dong, and W. Chen, "Role of tungsten oxide in inverted polymer solar cells" *Applied Physics Letters*, vol. 94, no. 4, p. 043311, 2009.
- [108] S. Han, W. S. Shin, M. Seo, D. Gupta, S.-J. Moon, and S. Yoo, "Improving performance of organic solar cells using amorphous tungsten oxides as an interfacial buffer layer on transparent anodes" *Organic Electronics*, vol. 10, no. 5, pp. 791-797, 2009.
- [109] Z. Tan, L. Li, C. Cui, Y. Ding, Q. Xu, S. Li, D. Qian, and Y. Li, "Solution-processed tungsten oxide as an effective anode buffer layer for high-performance polymer solar cells" *The Journal of Physical Chemistry C*, vol. 116, no. 35, pp. 18626-18632, 2012.
- [110] H. Choi, B. Kim, M. J. Ko, D.-K. Lee, H. Kim, S. H. Kim, and K. Kim, "Solution processed WO₃ layer for the replacement of PEDOT:PSS layer in organic photovoltaic cells" *Organic Electronics*, vol. 13, no. 6, pp. 959-968, 2012.
- [111] T. Stubhan, N. Li, N. A. Luechinger, S. C. Halim, G. J. Matt, and C. J. Brabec, "High fill factor polymer solar cells incorporating a low temperature solution processed WO₃ hole extraction layer" *Advanced Energy Materials*, vol. 2, no. 12, pp. 1433-1438, 2012.
- [112] R. Lampande, G. W. Kim, J. Boizot, Y. J. Kim, R. Pode, and J. H. Kwon, "A highly efficient transition metal oxide layer for hole extraction and transport in inverted polymer bulk heterojunction solar cells" *Journal of Materials Chemistry A*, vol. 1, no. 23, pp. 6895-6900, 2013.
- [113] Z. Zheng, Q. Hu, S. Zhang, D. Zhang, J. Wang, S. Xie, R. Wang, Y. Qin, W. Li, L. Hong, N. Liang, F. Liu, Y. Zhang, Z. Wei, Z. Tang, T. P. Russell, J. Hou, and H. Zhou, "A highly efficient non-fullerene organic solar cell with a fill factor over 0.80 enabled by a fine-tuned hole-transporting layer" *Advanced Materials*, vol. 30, no. 34, p. 1801801, 2018.
- [114] Y. Sun, C. J. Takacs, S. R. Cowan, J. H. Seo, X. Gong, A. Roy, and A. J. Heeger, "Efficient, Air-stable bulk heterojunction polymer solar cells using MoOx as the anode interfacial layer" *Advanced Materials*, vol. 23, no. 19, pp. 2226-2230, 2011.
- [115] S. Chen, C. E. Small, C. M. Amb, J. Subbiah, T. Lai, S.-W. Tsang, J. R. Manders, J. R. Reynolds, and F. So, "Inverted Polymer Solar Cells with Reduced Interface Recombination" *Advanced Energy Materials*, vol. 2, no. 11, pp. 1333-1337, Nov. 2012.
- [116] S. Murase, and Y. Yang, "Solution processed MoO₃ Interfacial layer for organic photovoltaics prepared by a facile synthesis method" *Advanced Materials*, vol. 24, no. 18, pp. 2459-2462, 2012.
- [117] Z. Tan, D. Qian, W. Zhang, L. Li, Y. Ding, Q. Xu, F. Wang, and Y. Li, "Efficient and stable polymer solar cells with solution-processed molybdenum oxide interfacial layer" *Journal of Materials Chemistry A*, vol. 1, no. 3, pp. 657-664, 2012.
- [118] K. Zilberberg, H. Gharbi, A. Behrendt, S. Trost, and T. Riedl, "Low-temperature, solution-processed MoOx for efficient and stable organic solar cells" *ACS Applied Materials & Interfaces*, vol. 4, no. 3, pp. 1164-1168, 2012.
- [119] S. R. Hammond, J. Meyer, N. E. Widjonarko, P. F. Ndione, A. K. Sigdel, A. Garcia, A. Miedaner, M. T. Lloyd, A. Kahn, D. S. Ginley, J. J. Berry, and D. C. Olson, "Low-temperature, solution-processed molybdenum oxide hole-collection layer for organic photovoltaics" *Journal of Materials Chemistry*, vol. 22, no. 7, p. 3249, 2012.
- [120] T. Stubhan, T. Ameri, M. Salinas, J. Krantz, F. Machui, M. Halik, and C. J. Brabec, "High shunt resistance in polymer solar cells comprising a MoO₃ hole extraction layer processed from nanoparticle suspension" *Applied Physics Letters*, vol. 98, no. 25, p. 253308, 2011.
- [121] Z. Yi Wang, S.-H. Lee, D.-H. Kim, J.-H. Kim, and J.-G. Park, "Effect of NiOx thin layer fabricated by oxygen-plasma treatment on polymer photovoltaic cell" *Solar Energy Materials and Solar Cells*, vol. 94, no. 10, pp. 1591-1596, 2010.
- [122] M. D. Irwin, D. B. Buchholz, A. W. Hains, R. P. H. Chang, and T. J. Marks, "p-Type semiconducting nickel oxide as an efficiency-enhancing anode interfacial layer in polymer bulk-heterojunction solar cells" *Proceedings of the National Academy of Sciences*, vol. 105, no. 8, pp. 2783-2787, 2008.
- [123] S.-Y. Park, H.-R. Kim, Y.-J. Kang, D.-H. Kim, and J.-W. Kang, "Organic solar cells employing magnetron sputtered p-type nickel oxide thin film as the anode buffer layer" *Solar Energy Materials and Solar Cells*, vol. 94, no. 12, pp. 2332-2336, 2010.
- [124] K. X. Steirer, J. P. Chesin, N. E. Widjonarko, J. J. Berry, A. Miedaner, D. S. Ginley, and D. C. Olson, "Solution deposited NiO thin-films as hole transport layers in organic photovoltaics" *Organic Electronics*, vol. 11, no. 8, pp. 1414-1418, 2010.
- [125] B. Mustafa, J. Griffin, A. S. Alsulami, D. G. Lidzey, and A. R. Buckley, "Solution processed nickel oxide anodes for organic photovoltaic devices" *Applied Physics Letters*, vol. 104, no. 6, p. 063302, 2014.
- [126] Z. Zhai, X. Huang, M. Xu, J. Yuan, J. Peng, and W. Ma, "Greatly reduced processing temperature for a solution-processed NiOx buffer layer in polymer solar cells" *Advanced Energy Materials*, vol. 3, no. 12, pp. 1614-1622, 2013.

- [127] S. Bai, M. Cao, Y. Jin, X. Dai, X. Liang, Z. Ye, M. Li, J. Cheng, X. Xiao, Z. Wu, Z. Xia, B. Sun, E. Wang, Y. Mo, F. Gao, and F. Zhang, "Low-temperature combustion-synthesized nickel oxide thin films as hole-transport interlayers for solution-processed optoelectronic devices" *Advanced Energy Materials*, vol. 4, no. 6, p. 1301460, 2014.
- [128] J. Zhang, J. Wang, Y. Fu, B. Zhang, and Z. Xie, "Efficient and stable polymer solar cells with annealing-free solution-processible NiO nanoparticles as anode buffer layers" *The Journal of Physical Chemistry C*, vol. 2, no. 39, pp. 8295-8302, 2014.
- [129] X. Liang, Q. Yi, S. Bai, X. Dai, X. Wang, Z. Ye, F. Gao, F. Zhang, B. Sun, and Y. Jin, "Synthesis of unstable colloidal inorganic nanocrystals through the introduction of a protecting ligand" *Nano Letters*, vol. 14, no. 6, pp. 3117-3123, 2014.
- [130] F. Jiang, W. C. H. Choy, X. Li, D. Zhang, and J. Cheng, "Post-treatment-free solution-processed non-stoichiometric NiO(x) nanoparticles for efficient hole-transport layers of organic optoelectronic devices" *Advanced Materials*, vol. 27, no. 18, pp. 2930-2937, 2015.
- [131] A. Singh, S. K. Gupta, and A. Garg, "Inkjet printing of NiO films and integration as hole transporting layers in polymer solar cells" *Scientific Reports*, vol. 7, 2017.
- [132] Q. He, K. Yao, X. Wang, X. Xia, S. Leng, and F. Li, "Room-Temperature and solution-processable cu-doped nickel oxide nanoparticles for efficient hole-transport layers of flexible large-area perovskite solar cells" *ACS Applied Materials & Interfaces*, vol. 9, no. 48, pp. 41887-41897, 2017.
- [133] J. Zheng, L. Hu, J. S. Yun, M. Zhang, C. F. J. Lau, J. Bing, X. Deng, Q. Ma, Y. Cho, W. Fu, C. Chen, M. A. Green, S. Huang, and A. W. Y. Ho-Baillie, "Solution-processed, silver-doped niOx as hole transporting layer for high-efficiency inverted perovskite solar cells" *ACS Applied Energy Materials*, vol. 1, no. 2, pp. 561-570, 2018.
- [134] R. Alkarsifi, Y. A. Avalos-Quiroz, P. Perkhun, X. Liu, M. Fahlman, A. K. Bharwal, C. M. Ruiz, D. Duché, J.-J. Simon, C. Videlot-Ackermann, O. Margeat, and J. Ackermann, "Organic-inorganic doped nickel oxide nanocrystals for hole transport layers in inverted polymer solar cells with color tuning" *Materials Chemistry Frontiers*, vol. 5, no. 1, pp. 418-429, 2020.